**AMERICAN SOCIETY FOR MICROBIOLOGY** | **Antimicrobial Agents and Chemotherapy**®

Check for updates

# Telmisartan Restricts Chikungunya Virus Infection *In Vitro* and *In Vivo* through the AT1/PPAR-γ/MAPKs Pathways

Saikat De,[a,b] Prabhudutta Mamidi,[a] Soumyajit Ghosh,[a,b] Supriya Suman Keshry,[a,c] Chandan Mahish,[d] Sweta Smita Pani,[a] Eshna Laha,[a,b] Amrita Ray,[a,b] Ankita Datey,[a,c] Sanchari Chatterjee,[a,b] Sharad Singh,[a,c] Tathagata Mukherjee,[d] Somlata Khamaru,[d] Subhasis Chattopadhyay,[d] Bharat Bhusan Subudhi,[e] Soma Chattopadhyay[a]

aInstitute of Life Sciences, Bhubaneswar, India
bRegional Centre for Biotechnology, Faridabad, India
cSchool of Biotechnology, Kalinga Institute of Industrial Technology (KIIT) University, Bhubaneswar, India
dSchool of Biological Sciences, National Institute of Science Education and Research, HBNI, Bhubaneswar, India
eSchool of Pharmaceutical Sciences, Siksha O Anusandhan Deemed to be University, Bhubaneswar, India

Prabhudutta Mamidi and Soumyajit Ghosh contributed equally to this work; author order was determined by seniority.

**ABSTRACT** Chikungunya virus (CHIKV) has reemerged as a global public health threat. The inflammatory pathways of the renin-angiotensin system (RAS) and peroxisome proliferator-activated receptor-gamma (PPAR-γ) are usually involved in viral infections. Thus, telmisartan (TM), which is known to block the angiotensin 1 (AT1) receptor and activate PPAR-γ, was investigated for activity against CHIKV. The anti-CHIKV effect of TM was investigated *in vitro* (Vero cells, RAW 264.7 cells, and human peripheral blood mononuclear cells [hPBMCs]) and *in vivo* (C57BL/6 mice). TM was found to abrogate CHIKV infection efficiently (50% inhibitory concentration ($IC_{50}$) of 15.34 to 20.89 $\mu$M in the Vero cells and RAW 264.7 cells, respectively). Viral RNA and proteins were reduced remarkably. Additionally, TM interfered in the early and late stages of the CHIKV life cycle with efficacy during pretreatment and posttreatment. Moreover, the agonist of the AT1 receptor and an antagonist of PPAR-γ increased CHIKV infection, suggesting that the antiviral potential of TM occurs through modulating host factors. In addition, reduced activation of all major mitogen-activated protein kinases (MAPKs), NF-κB (p65), and cytokines by TM occurred through the inflammatory axis and supported the fact that the anti-CHIKV efficacy of TM is partly mediated through the AT1/PPAR-γ/MAPKs pathways. Interestingly, at a human equivalent dose, TM abrogated CHIKV infection and inflammation significantly, leading to reduced clinical scores and complete survival of C57BL/6 mice. Additionally, TM reduced infection in hPBMC-derived monocyte-macrophage populations *in vitro*. Hence, TM was found to reduce CHIKV infection by targeting both viral and host factors. Considering its safety and *in vivo* efficacy, it can be a suitable candidate in the future for repurposing against CHIKV.

**KEYWORDS** Chikungunya virus, telmisartan, AT1, PPAR-γ, drug repurposing

Chikungunya virus (CHIKV) infection is categorized as a neglected tropical disease by WHO. However, in the last 2 decades, CHIKV has reemerged and spread globally (1–4). CHIKV is an alphavirus that is transmitted to humans by the *Aedes* sp. of mosquitoes. The most common symptoms include fever, nausea, headaches, rash, and polyarthralgia. While the acute symptoms subside gradually, polyarthritis persists and may last for 90 days (5–8). Further, it is also known to cause neurological complications that lead to irreversible brain damage (9). In the presence of comorbidities and in vulnerable people, CHIKV infection can cause severe complications and death (10). Although mortality was underestimated (11) between 2014 and 2017, more than 35,000 deaths were associated with CHIKV infection across American and Caribbean regions (3). Because no potent vaccine or drugs are available

to date, extensive efforts are being taken to develop an antiviral strategy for early clinical application (12, 13).

Drug repurposing is a strategy to find new clinical applications of the existing drugs with minimum cost, time, and risk (14). Although some drugs, including chloroquine and ribavirin, have been repurposed against CHIKV, their therapeutic benefits are limited (13). Thus, there is a need for investigations that find new drugs to reposition against CHIKV. Angiotensin II (Ang II) mediated activation of the AT1 receptor in the renin-angiotensin system (RAS) is a primary mediator of oxidative stress and inflammation (15, 16). Its involvement in viral infection was first reported with improved survival of DBA/2 mice against encephalomyocarditis (EMC) virus infection following administration of Ang II inhibitors (17). Since then, it has been clinically correlated with viral diseases, including influenza virus (18), bunyavirus (19), Dengue virus (DENV) (20), coxsackievirus (21), Ebola virus (22), western equine encephalitis virus, and a neuro-adapted Sindbis virus (23). Considering the effects of Ang II inhibitors against some of these alphaviruses, AT1 blocking drugs may be expected to be effective against CHIKV. Because CHIKV also affects the central nervous system (CNS) (24), it is desirable to use an AT1 blocker that can cross the blood-brain barrier. Only telmisartan (TM) is known to have good brain permeability among this category of drugs (24). Our preliminary investigations suggested the anti-CHIKV potential of TM (Indian Patent Application no. 201931012926, status: not published; filing date: 30/03/2019). Recently, Tripathi et al. (25) corroborated this by demonstrating the direct inhibition of the CHIKV nonstructural protein P2 (nsP2) protease activity and CHIKV infection *in vitro*. Thus, TM can be a potential drug for repurposing against CHIKV infection.

To justify the potential of TM for repurposing against CHIKV, the current investigation was carried out to understand its mode of action and effects *in vitro* and *in vivo* in mice. It was also investigated against different strains of CHIKV to justify its broad anti-CHIKV potential. The mode of action was investigated by looking at its impact on the levels of CHIKV RNA and proteins. Moreover, the interference in different phases of the CHIKV life cycle was assessed. Finally, the effects were validated in the preclinical model in C57BL/6 mice using human equivalent doses (26) and in hPBMC-derived monocyte-macrophage cells.

## RESULTS

**TM inhibits CHIKV infection efficiently.** To determine the cytotoxicity of TM, a 3-(4,5-dimethylthiazol-2-yl)-2,5-diphenyl tetrazolium bromide (MTT) assay was performed. At 300 $\mu$M TM, viability of the Vero and RAW 264.7 cells was found to be 100% and >90%, respectively (Fig. 1A and 1F). Thus, a dose of 100 $\mu$M or less was used in further investigations. To observe the effect of TM on reducing the cytopathic effect (CPE), confluent Vero cells were infected with CHIKV Prototype strain (PS) at a multiplicity of infection (MOI) of 0.1. After 18 h post-infection (pi), a remarkable decrease in the CPE was observed in cells treated with TM (30, 50, 70, or 100 $\mu$M) compared to the control (Fig. 1B). This anti-CHIKV potential was also evident in a subsequent study using confocal microscopy, which showed a significant reduction in viral antigen E2 in a dose-dependent manner (Fig. 1C and D). The IC$_{50}$ of TM was found to be 15.34 $\mu$M (Fig. 1E) and 20.89 $\mu$M (Fig. 1G) against the CHIKV prototype strain (PS) and CHIKV Indian strain (IS), respectively. Hence, the data suggest a significant inhibitory capacity of TM in inhibiting CHIKV infection *in vitro*.

**TM reduces viral RNA and protein levels.** To confirm the effect of TM on CHIKV structural (E1/E2) and nonstructural (nsP2) RNAs from virus-infected and TM-treated cells, qRT-PCR was conducted with respective primers (Table S1). At 100 $\mu$M in CHIKV-PS infected Vero cells, TM reduced the CHIKV E1 and CHIKV nsP2 RNA levels by 25-fold and 5-fold, respectively (Fig. S1A). Similar reductions of 90-fold and 45-fold were observed in CHIKV-IS-infected RAW 264.7 cells in the presence of 70 $\mu$M TM (Fig. S1B). Further, viral protein levels were estimated by Western blots and flow cytometry. At 100 $\mu$M in CHIKV-PS infected Vero cells, TM reduced the nsP2 and E2 protein levels by 86% and 95%, respectively (Fig. 2A and B and Fig. S2A and B). In CHIKV-IS infected RAW 264.7 cells, TM (70 $\mu$M) reduced the nsP2 and E2 protein levels by 75% and 88%, respectively (Fig. 2E and F and Fig. S2C and D). Thus, it could be suggested that TM inhibits CHIKV infection by reducing viral RNAs and proteins.
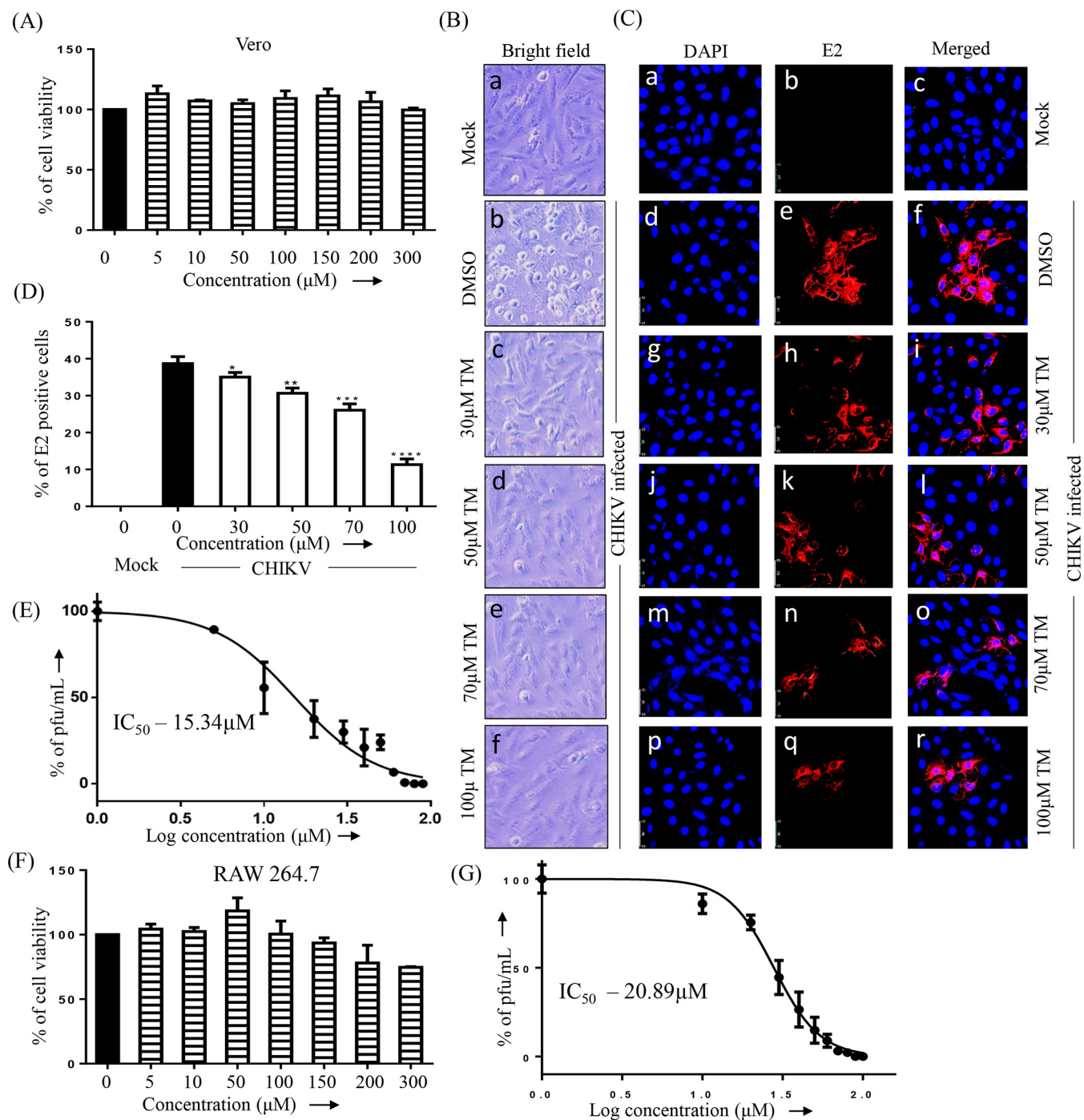
FIG 1 Telmisartan inhibits CHIKV infection efficiently. (A) Bar diagram showing the viability of Vero cells in the presence of different concentrations of TM. (B) Vero cells plated onto the coverslips were infected with CHIKV-PS and TM was added at different concentrations (30 $\mu$M, 50 $\mu$M, 70 $\mu$M, or 100 $\mu$M). CPE was observed under a microscope at 18 h pi for the uninfected and infected Vero cells after drug treatment, and pictures were taken with 20× magnification in a bright field microscope. (C) After 18 h pi, the cells were fixed and stained with an E2 antibody followed by a secondary antibody, anti-mouse Alexa Fluor 594 (red). Nuclei were counterstained with DAPI (blue). (D) Bar diagram representing the percent positive E2 cell counts from the confocal images. (E) Vero cells were infected with CHIKV-PS and TM was added at different concentrations (10 $\mu$M, 20 $\mu$M, 30 $\mu$M, 40 $\mu$M, 50 $\mu$M, 60 $\mu$M, 70 $\mu$M, 80 $\mu$M, 90 $\mu$M, or 100 $\mu$M). The supernatants were collected at 18 h pi, and virus titers were determined by plaque assay. The $IC_{50}$ of TM in CHIKV-PS infected Vero cells is noted. The x-axis depicts the logarithmic value of the different concentrations of TM, and the y-axis depicts the percentage of PFU/ml. (F) Bar diagram showing the viability of RAW 264.7 cells in the presence of different concentrations of TM. (G) RAW 264.7 cells were infected with CHIKV-IS and TM was added at different concentrations (10 $\mu$M, 20 $\mu$M, 30 $\mu$M, 40 $\mu$M, 50 $\mu$M, 60 $\mu$M, 70 $\mu$M, 80 $\mu$M, 90 $\mu$M, or 100 $\mu$M). The supernatants were collected at 8 h pi, and virus titers were determined by plaque assay. The $IC_{50}$ of TM in CHIKV-IS infected RAW 264.7 cells. The x-axis and y-axis are the same as in (E). Data represented as mean $\pm$ SE (n = 3; $P \leq 0.05$ was considered statistically significant).
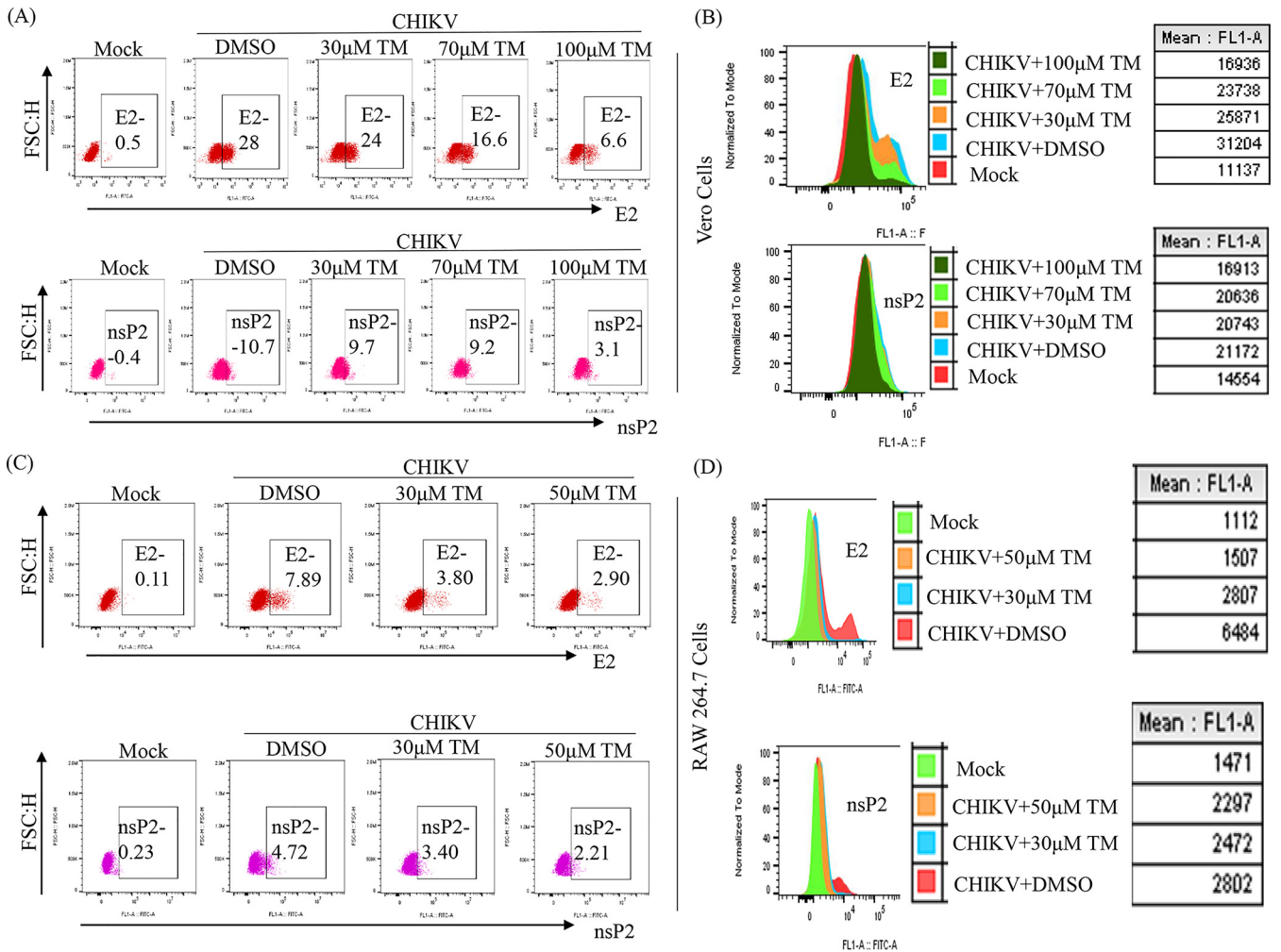
**FIG 2** Reduction of CHIKV protein after TM treatment. Vero cells and RAW 264.7 cells were infected with CHIKV and treated with different concentrations of TM as mentioned in Fig. 1. Vero cells were harvested at 18 h pi, and RAW 264.7 cells were harvested at 8 h pi. After that, both cells were stained with CHIKV nsP2 and E2 antibodies and analyzed by flow cytometry. (A and C) Dot plot analysis showing percent cells positive for E2 and nsP2 against FSC-H (forward scatter height) for Vero and RAW 264.7 cells, respectively. (B and D) Histogram and table showing mean fluorescent intensities (MFI) of E2 and nsP2 proteins. Data represented as mean $\pm$ SE ($n = 3$; $P \leq 0.05$ was considered statistically significant).

**TM interferes in the early and late stages of the CHIKV life cycle.** To understand which stage of the CHIKV life cycle was affected by TM, a "time-of-addition" experiment was performed. The estimated viral titers showed that the release of infectious virus particles was abrogated with the addition of TM at 0 to 10 h pi by 82 to 95% compared to control (Fig. 3A). Even after the addition of TM at 12 to 16 h pi, the abrogation of infectious virus particle release was 45 to 75%. The positive control (Ribavirin), which is well known for interfering in the early phase of the CHIKV life cycle, exhibited a 70 to 88% decrease in the release of infectious virus particles when it was added at 0 to 6 h pi. However, this was reduced (from 10% to 0%) compared to the infection control when the treatment was added at 12 to 16 h pi (Fig. 3A). Therefore, it can be concluded that TM might interfere in both the early and late stages of the CHIKV life cycle.

**Pretreatment and posttreatment with TM significantly reduced CHIKV infection.** To evaluate the effectiveness of various treatment regimens, TM (50 $\mu$M) was administered at different stages of infection. The results revealed that viral particle formation was abrogated by 30 to 40% following pretreatment with TM (Fig. 3B) whereas little (3 to 4%) to almost no inhibition was found when TM was used during infection. Compared to these conditions, TM was more effective in the postinfection stage with a 55 to 64% reduction in virus particle formation. Interestingly, a 65 to 70% reduction was observed when the cells were treated with TM before and during the infection. However, it was most effective when added

(A)



(B)
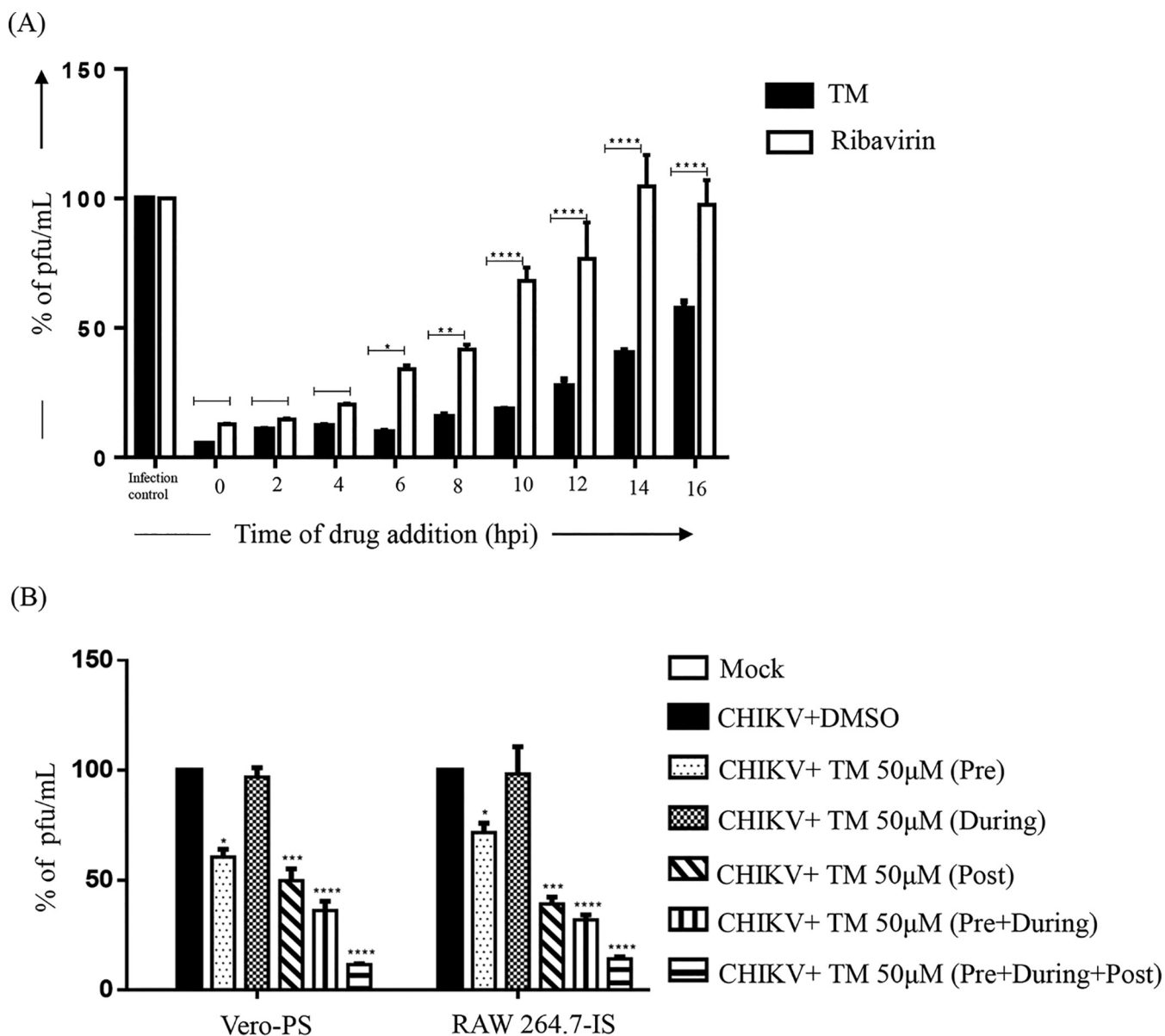


**FIG 3** TM interferes in the early and late stages of the CHIKV life cycle, and pretreatment and posttreatment of TM significantly reduce CHIKV infection. (A) Vero cells were infected by CHIKV-PS at a MOI of 0.1 and 100 $\mu$M TM was added to each sample every 2 h up to 16 h pi. Ribavirin (10 $\mu$M) was used as a control. The bar diagram represents the percentage of virus for all the samples from the supernatants that were collected at 18 h pi. (B) Vero and RAW 264.7 cells were treated with TM (50 $\mu$M) separately before (3 h before infection), during (1.5 h during infection), and postinfection (for 18 h in case of Vero cells and 8 h in case of RAW264.7 cells). The drug was present before and during infection for the pretreatment condition. The drug was present before, during, and after infection for before + during + after infection condition. Supernatants collected at 18 h pi for Vero and 8 h pi for RAW 264.7 cells were analyzed by plaque assay. The bar diagram shows the percentage of the virus particle. Data presented as mean ± SE ($n = 3$; $P \leq 0.05$ was considered statistically significant).

preinfection, during the infection, and postinfection with 87 to 90% abrogation of viral particle formation. The data suggest that TM might not affect the attachment process. Nevertheless, the presence of TM in all the phases demonstrated the best effectiveness against CHIKV.

**Inhibition of CHIKV by TM is mediated through AT1 and PPAR-$\gamma$ pathways.** As TM is a modulator of AT1 and PPAR-$\gamma$ (20, 27), these host factors might have roles in its anti-CHIKV property. Thus, an agonist of AT1 (AG) and an antagonist of PPAR-$\gamma$ (GW9662 [GW]) were used in this study. GW and AG were nontoxic at concentrations of 20 $\mu$M (Fig. S3A and B) and 100 $\mu$M (Fig. S3C and D), respectively. Without infection, AG was found to upregulate AT1 protein levels in a dose-dependent manner in both the cell lines (Fig. S4A, B, C), whereas GW did not affect the PPAR-$\gamma$ protein level significantly (Fig. S4D, E, F) because it is a functional inhibitor (28, 29). Their treatment before

and after viral infection revealed that both GW (Fig. S3E and F) and AG (Fig. S3G and H) dose-dependently augmented viral particle formation with upregulation of the CHIKV E2 and nsP2 protein levels (Fig. S3I and J). Subsequently, this increased the CPE and level of E2 protein (Fig. 4A). This was associated with enhanced CHIKV progeny release in the presence of both GW (25% in Vero and 35% in RAW 264.7 cells; Fig. 4B and C) and AG (42% in Vero and 105% in RAW 264.7 cells; Fig. 4B and C). Although a significant increase in the levels of CHIKV E2 and nsP2 were observed with both GW and AG (Fig. 5A, B, E, and F), the levels were higher following AG treatment. (Fig. 5A, B, E, F). In contrast, TM treatment significantly reduced infection and levels of CHIKV proteins (Fig. 5A, B, E, F). While AT1 protein levels were upregulated by 15 to 20% upon infection, TM treatment downregulated this by 53 to 74% (Fig. 5A, C, E, G). On the other hand, there was downregulation (30 to 70%) of PPAR-$\gamma$ in infected cells, and TM treatment augmented the PPAR-$\gamma$ expression by 140 to 300% (Fig. 5A, D, E, H). To strengthen this observation, an established PPAR-$\gamma$ agonist Rosiglitazone (Rosi) was tested against CHIKV. At a nontoxic dose of 200 $\mu$M (Fig. S5A), it showed 93% inhibition of viral particle formation (Fig. S5C), 60% upregulation of PPAR-$\gamma$, and a reduction in the CHIKV E2 (86%) and CHIKV nsP2 (80%) protein levels (Fig. S5D and E). Further, a transcriptional PPAR-$\gamma$ inhibitor, T0070907 (T007) (28), at a nontoxic concentration (Fig. S5B) of 20 $\mu$M increased CHIKV particle formation by 35% (Fig. S5F) and increased CHIKV E2 (62%) and CHIKV nsP2 (51%) protein levels (Fig. S5G and H). Taken together, it could be suggested that the activation of the AT1 receptor and blocking of PPAR-$\gamma$ have contributed to the enhancement of viral infection. Thus, the anti-CHIKV effect of TM can be mediated through these host factors.

**AT1 agonist (AG) and PPAR-$\gamma$ antagonist (GW) mediated augmentation of CHIKV infection is also inhibited by TM.** To understand the ability of TM to abrogate CHIKV infection that was augmented by AG or GW, RAW 264.7 cells were treated with AG or GW along with TM before and after CHIKV-IS infection. Interestingly, TM reduced infection by 80% and 70% when cotreated with GW or AG, respectively (Fig. 6A). It also reduced the nsP2 protein level (85% in the presence of GW and 75% in the presence of AG; Fig. 6B and C). The increase in the level of AT1 in the presence of AG and the decrease in the level of PPAR-$\gamma$ in the presence of GW was antagonized by TM with a reduction in AT1 and enhancement in PPAR-$\gamma$ levels (Fig. 6D and E). These results further support that the antiviral activity of TM is partly mediated through AT1 and PPAR-$\gamma$.

**TM reduces the CHIKV-induced inflammatory response through the MAPK pathway, NF-$\kappa$B, and COX-2.** To find out whether TM modulates CHIKV-induced inflammation, induction of p38, extracellular signal-regulated kinase 1/2 (ERK1/2), Jun N-terminal protein kinase (JNK), cJUN, interferon regulatory factor 3 (IRF3), NF-$\kappa$B, cyclooxygenase-2 (COX-2), tumor necrosis factor-alpha (TNF-$\alpha$) and interleukin-6 (IL-6) were estimated. Compared to mock, the CHIKV infection led to 2 to 3-fold induction in the phosphorylation of each of the major MAPKs: p38, ERK1/2, and JNK. However, treatment with TM resulted in reduced phosphorylation, whereas MAPKs were activated 2.5 to 4-fold in infected cells compared to mock in the presence of AG and GW (Fig. 7A to D). Phosphorylation of cJUN is one of the major transcription factors for the expression of proinflammatory cytokines (30). Its induction was 10-fold higher after infection. While TM treatment reduced the level of cJUN by 2-fold, GW and AG increased it by 1.5-fold and 1.8-fold, respectively (Fig. 7A and E). Furthermore, TM treatment reduced the expressions of another key transcription factor, p-IRF3, by 2-fold compared to the infection control, whereas this level was observed to be 1.6-fold and 1.7-fold higher during GW and AG treatment, respectively, compared to that during infection (Fig. 7A and F). Similarly, induction of p-NF-$\kappa$B (p65) was downregulated by 2-fold in the presence of TM but upregulated with GW and AG compared to infection (Fig. 7A and G). In addition, the expression of COX-2, a key enzyme that mediates prostaglandin synthesis (31), was downregulated by TM (2-fold); however, it was upregulated by GW and AG compared to infection (Fig. 7J and K). TM treatment was also able to inhibit levels of cytokines significantly (TNF-$\alpha$ by 2.9-fold and IL-6 by 10-fold; Fig. 7L and M). On the other hand, AG and GW treatment increased the levels of TNF-$\alpha$ and IL-6 (data not shown). Altogether, reduction in the activation of all major MAPKs and cytokines by TM through the MAPK inflammatory axis supports its anti-CHIKV property
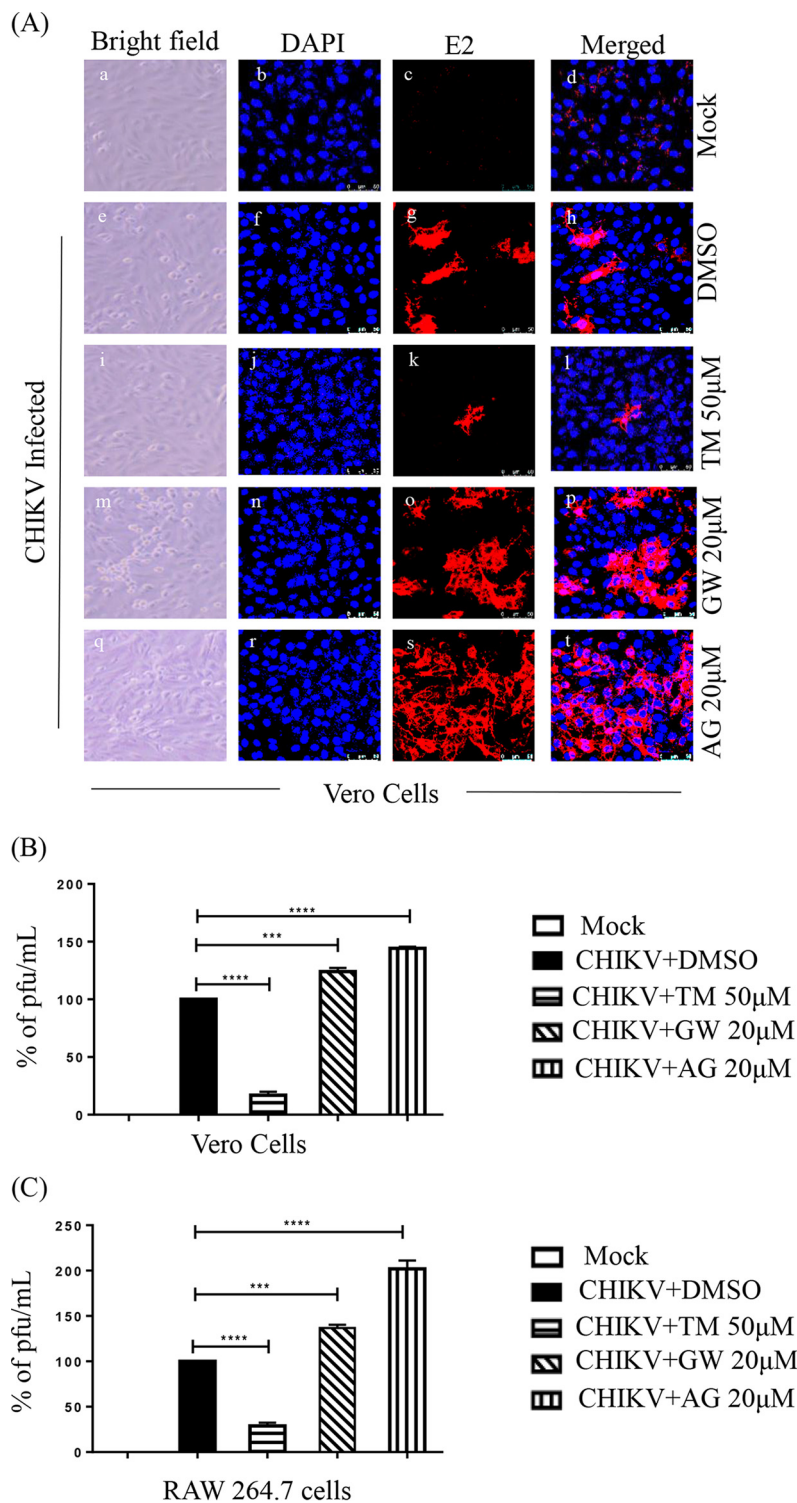
**FIG 4** AT1 and PPAR-$\gamma$ can modulate CHIKV infection. (A) Vero cells plated onto the coverslips were treated with TM (50 $\mu$M), GW (20 $\mu$M), or AG (20 $\mu$M) individually before the infection for 3 h, infected with CHIKV-PS at a MOI of 0.1, and treated again with TM (50 $\mu$M), GW (20 $\mu$M), or AG (20 $\mu$M) individually. At 18 h pi, the cells were fixed and probed with E2 antibody followed by staining with secondary antibody, anti-mouse Alexa Fluor 594 (red). Nuclei were counterstained with DAPI (blue). (B) Bar diagrams depicting the percentage of viral titers in the collected supernatant. (C) RAW 264.7 cells were treated with TM (50 $\mu$M), GW (20 $\mu$M), and AG (20 $\mu$M), infected with CHIKV-IS at a MOI of 5, and again treated with TM (50 $\mu$M), GW (20 $\mu$M), and AG (20 $\mu$M). Bar diagrams indicate the percentage of viral titer in the cell supernatant.

that is partly mediated through the AT1/PPAR-$\gamma$/MAPKs pathways. Furthermore, down-regulation of p-NF-$\kappa$B and COX-2 indicates the anti-inflammatory effect of TM.

**TM protects mice from CHIKV infection and inflammation.** The anti-CHIKV effect of TM was assessed in C57BL/6 mice infected with CHIKV-PS following treatment with TM (10 mg/kg) at 12 h intervals up to 5 or 6 d pi. The infected mice showed symptoms of arthritis in their limbs and impaired mobility, whereas TM-treated animals showed no such abnormalities (Fig. 8A). Based on the viral RNA isolated from the serum of animals, the CHIKV RNA copy number was reduced by 55% with TM (Fig. 8B). In muscles, reductions in CHIKV E1 RNA (4-fold) and in CHIKV E2 protein (62%) were observed (Fig. 8C to E). Similarly, a reduction of E1 RNA was detected in other organs, such as the liver (5-fold), kidney (10-fold), and spleen (100-fold). The protein levels of CHIKV E2 were also reduced in the liver (40%), kidney (66%), and spleen (75%). Further, infected muscle sections stained with hematoxylin and eosin (H&E) showed large infiltration of the mononuclear lymphocytes (Fig. 8F a-II), which was remarkably lower after TM treatment (Fig. 8F a-III). Additionally, immunohistochemistry (IHC) analysis revealed the reduction of E2 level in CHIKV infected muscle upon TM treatment (Fig. 8F b: VII-IX). Further, it was found that different cytokines and chemokines like IL-12 (p40), monocyte chemoattractant protein 1 (MCP-1), IL-6, interferon gamma-induced protein 10 (IP-10), keratinocyte chemoattractant (KC), RANTES, granulocyte-macrophage colony-stimulating factor (GM-CSF), macrophage inflammatory protein 1$\beta$ (MIP-1$\beta$), and TNF-$\alpha$ which are known to be associated with CHIKV infection (32) were reduced significantly in the mice serum by TM (Fig. 8I, J and K). To further confirm the *in vivo* efficacy of TM on CHIKV infection, the survival curve was analyzed. All the CHIKV infected mice died on the 8th day postinfection, whereas TM treatment alleviated symptoms and provided complete protection to all the animals (Fig. 8G and H). These results indicate that TM protects mice against CHIKV infection and inflammation.

**TM reduces CHIKV infection in hPBMC-derived monocyte-macrophage populations *in vitro*.** The data indicate the regulatory effect of TM against CHIKV in an epithelial cell line (Vero) and a mouse-derived monocyte-macrophage cell line (RAW 264.7) *in vitro* as well as in a mouse model. Hence, it was interesting to investigate the possible effect of TM against CHIKV infection in a higher-order mammalian system and human peripheral blood mononuclear cell (hPBMC)-derived monocyte-macrophage cells (enriched with CD14$^+$/CD11b$^+$ cell populations). Immunologic characterization of hPBMC-derived adherent cell populations was carried out by staining for specific markers of B cells (CD19), T cells (CD3), monocyte-macrophage cells (CD11b and CD14) and then analyzing by flow cytometry (Fig. 9A). It was observed that the adherent population was highly enriched with CD14$^+$CD11b$^+$ monocyte-macrophage cells (Fig. 9A), and TM was nontoxic up to 100 $\mu$M concentration (Fig. 9B). The hPBMC-derived monocyte-macrophage cells that were infected with CHIKV and treated with TM (100 $\mu$M) showed reduced CPE (Fig. 9C). The effect of TM was then analyzed using the hPBMC-derived monocyte-macrophage cells that were collected from 3 healthy donors after CHIKV infection. It was observed that the viral particle formation was reduced by 45% in CHIKV-infected hPBMCs in the presence of TM (Fig. 9D). The CHIKV-infected hPBMCs showed 21.13 $\pm$ 1.66% positivity for E2, whereas preincubation with TM for 3 h led to a 17.4 $\pm$ 0.7% decrease in E2 positive cells (Fig. 9E and F). Taken together, the data suggest that TM might abrogate CHIKV infection significantly in hPBMC-derived monocyte-macrophage populations *in vitro*.

## DISCUSSION

CHIKV has emerged as an infectious disease of global concern. Unfortunately, there is no effective antiviral with activity against CHIKV. This has pushed efforts for repurposing existing drugs against CHIKV. Because RAS and PPAR-$\gamma$ pathways are involved in the progress of viral infections, TM was investigated against CHIKV *in vitro* and *in vivo*.

It abrogated CHIKV infection efficiently in the Vero and RAW 264.7 cells with remarkable inhibition of the viral RNA and protein levels. Additionally, TM interfered in the early and late stages of the CHIKV life cycle and was found to be effective during pretreatment and post-treatment. Moreover, the AT1 receptor agonist and PPAR-$\gamma$ antagonist increased CHIKV infection that was antagonized by TM. Thus, the antiviral effect of TM could be partly mediated
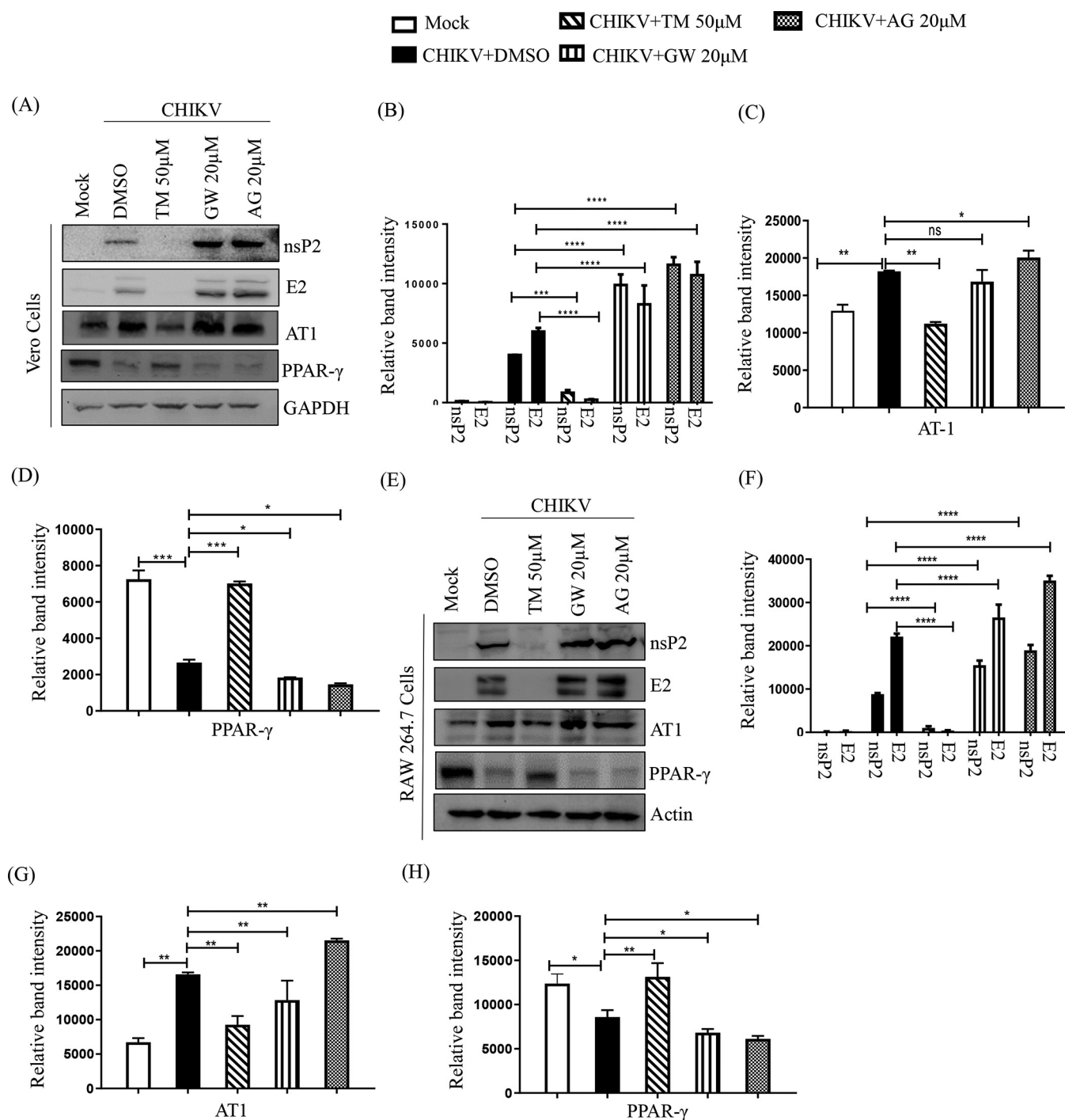
**FIG 5** Inhibition of CHIKV by TM is mediated through AT1 and PPAR-γ. Vero and RAW 264.7 cells were treated with TM (50 μM), GW (20 μM), and AG (20 μM) for 3 h before infection. The Vero cells were infected by CHIKV-PS (MOI of 0.1) and RAW 264.7 cells were infected by CHIKV-IS (MOI of 5). After 1.5 h incubation with the virus, cells were washed and again treated with TM (50 μM), GW (20 μM), and AG (20 μM). Cells were harvested at 18 h pi and 8 h pi for Vero cells and RAW264.7 cells, respectively. (A and E) Western blot showing the levels of different proteins (nsP2, E2, AT1, and PPAR-γ) in the infected cells. GAPDH and Actin were used as loading controls for Vero and RAW 264.7 cells, respectively. Bar diagram indicating the relative band intensities of viral (nsp2 and E2) and host (AT1 and PPAR-γ) protein levels in Vero (B to D) and RAW 264.7 cells (F to H). Data presented as mean ± SE. ($n = 3$; $P ≤ 0.05$ was considered statistically significant).

through these host factors. It also diminished the CHIKV-induced inflammatory responses. The reduced activation of all the major MAPKs and cytokines by TM occurred through MAPKs inflammatory axis and supported that the anti-CHIKV efficacy of TM was partly mediated through the AT1/PPAR-γ/MAPKs pathways. Further, at the human equivalent dose (26), TM abrogated CHIKV infection and inflammation *in vivo*, leading to reduced clinical scores
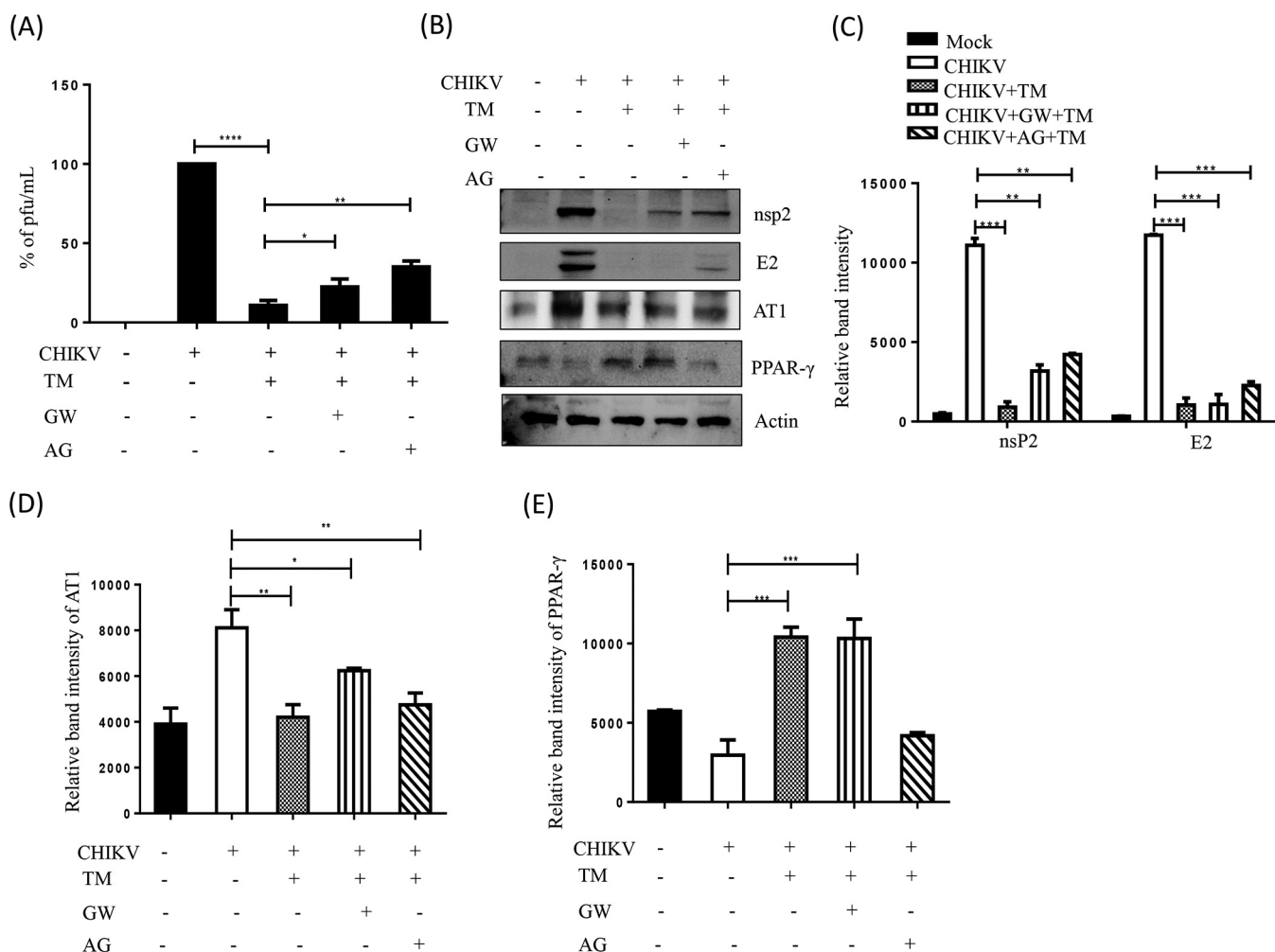
**FIG 6** TM abrogates AT1 agonist (AG) and PPAR-γ antagonist (GW) mediated enhanced CHIKV infection. RAW 264.7 cells were cotreated with TM (50 $\mu$M), GW (20 $\mu$M), and AG (20 $\mu$M) before and after CHIKV-IS infection at a MOI of 5. (A) Bar diagram indicating the percentage of viral titer in the cell supernatant. (B) Western blot showing the levels of different proteins (nsP2, E2, AT1, and PPAR-γ) in the infected cells. Actin was used as a loading control. Bar diagram indicating the relative band intensities of viral (nsp2 and E2) and host protein levels (AT1 and PPAR-γ) (C to E). Data presented as mean ± SE. ($n = 3$, $P \leq 0.05$ was considered statistically significant).

and survival of C57BL/6 mice (Fig. 10). Additionally, TM reduced infection in hPBMC-derived monocyte-macrophage populations *in vitro*.

Our preliminary findings suggested the inhibition potential of CHIKV by TM. Subsequently, Tripathi et al. (25) showed the inhibition of the CHIKV nsP2 protein by TM with a reduction in CHIKV infection. The present study showed its ability to inhibit CHIKV infection by reducing viral RNAs and proteins.

Moreover, the time-of-addition experiment also revealed that TM might interfere in both the early and late stages of the CHIKV life cycle. When used as a treatment during infection, there was no effect on viral particle formation. In contrast, pretreatment and posttreatment had greater effects than posttreatment only. Thus, TM might not have much effect on the viral attachment process, and it could be speculated that TM targets multiple phases of the CHIKV life cycle to modulate infection. However, this needs further investigation.

As TM is an established AT1 receptor blocker and partial agonist of PPAR-γ, modulation of these host factors might have a role in its antiviral efficacy. Thus, the AT1 receptor agonist (AG) and PPAR-γ antagonist (GW) were used to demonstrate the involvement of these host factors in the anti-CHIKV property of TM. Further, inhibition of CHIKV infection by PPAR-γ agonist (Rosi) as well as an increase in CHIKV infection by PPAR-γ inhibitor (T007) supported the PPAR-γ mediated anti-CHIKV effect of TM (Fig. 10).
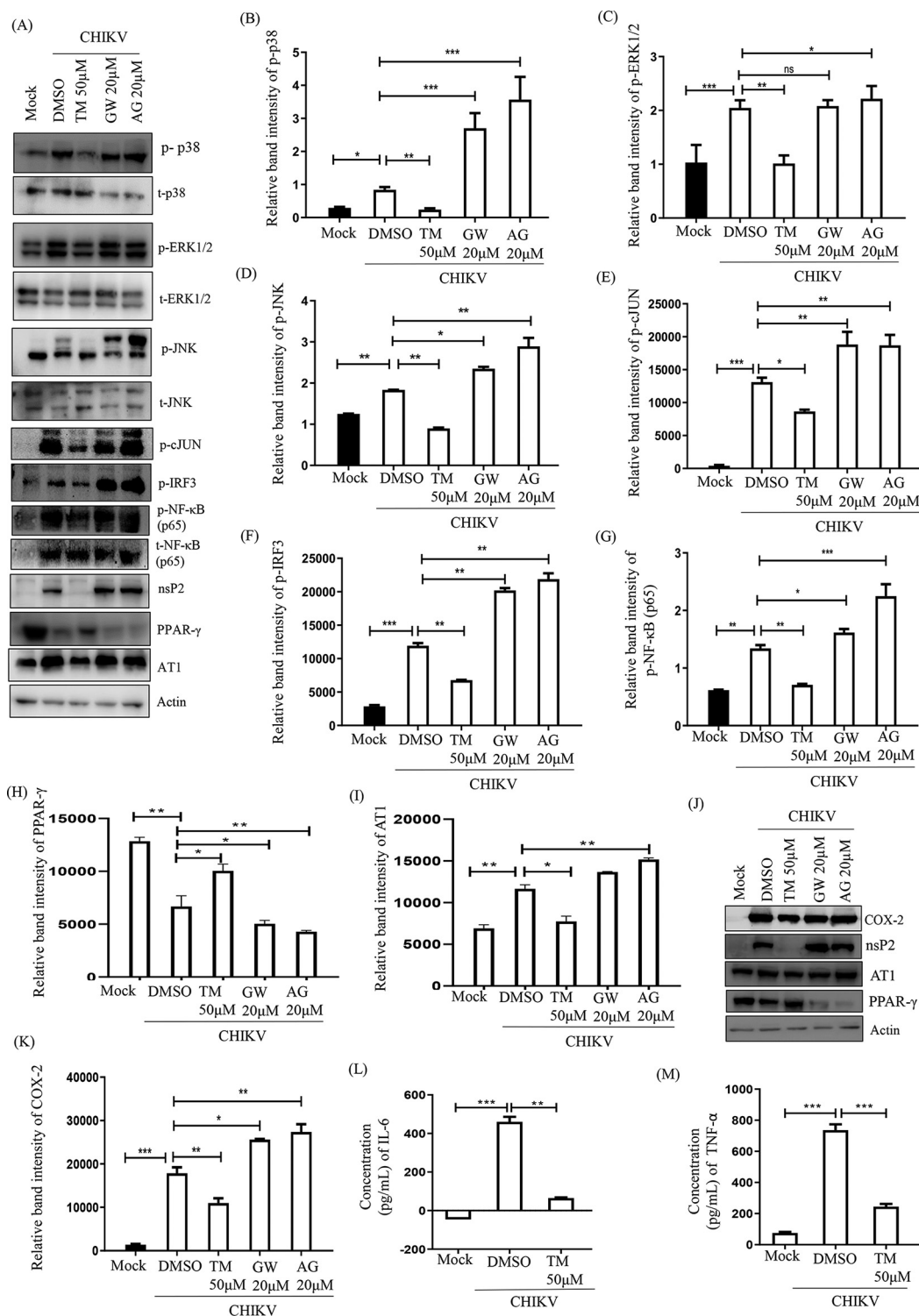
**FIG 7** TM reduces the CHIKV-induced inflammatory response through the MAPK pathway, NF-κB, and COX-2. RAW 264.7 cells were infected with CHIKV-IS, treated with TM (50 μM), GW (20 μM), and AG (20 μM) then harvested at 8 h pi. (A) Western blot showing the nsP2, PPAR-γ, and AT1 proteins levels along with phosphorylation status of p38, ERK, JNK, cJUN, IRF3, and NF-κB in RAW 264.7 cell lysates. Actin was used as a loading control. (B to I) Bar diagrams indicating relative band intensities of p-p38, p-ERK, p-JNK, p-cJUN, p-IRF3 p-NF-κB, PPAR-γ, and AT1 (J) Western blot showing the level of COX-2 protein. (K) Bar diagrams depicting relative band intensities of COX-2 protein. (L and M) Bar diagram showing the levels of secreted cytokines (TNF-α and IL-6) of CHIKV-infected and TM-treated macrophages in the supernatants quantified using sandwich ELISA of CHIKV-infected and TM-treated macrophages. Data represented mean ± SE ($n = 3$; $P \leq 0.05$ was considered statistically significant).

In agreement with these actions of TM, the downstream mediators were also found to be modulated. MAPKs are activated in CHIKV infection (33) and their inhibition has been shown to abrogate its infection (30). Accordingly, the phosphorylation of major MAPKs, including p38, ERK1/2, and JNK, was observed to be greater following infection. While AG and GW induced it further, TM reduced the activated MAPKs significantly. This corroborates that TM partly targets the AT1/PPAR-$\gamma$ axis to reduce CHIKV infection. Further, these axes and downstream mediators, including MAPKs are also responsible for the induction of chemokines and cytokines that are aggravating factors for arthritis. As a result, TM has been shown to reduce inflammation by regulating these mediators (34–37). Here, the induction of p-NF-$\kappa$B and COX-2 was significantly reduced by TM, whereas both AG and GW enhanced their expression. These inflammatory mediators have also been demonstrated to be involved in CHIKV-induced inflammation with elevated levels of IL-6 and TNF-$\alpha$ in CHIKV-infected macrophage cell lines (38). Cytokine levels are often associated with the severity of the viral infection (39). Accordingly, treatment with AG and GW increased the levels of TNF-$\alpha$ and IL-6, which were reduced remarkably after the treatment of TM. Because these axes are also mediators of the inflammatory process, TM can be expected to manage both infection and symptoms related to CHIKV (Fig. 10).

The *in vitro* findings were validated in the C57BL/6 mouse model. While infected mice showed symptoms of arthritis and immobility, TM (10 mg/kg; a human equivalent dose of 40 mg [26]) alleviated these symptoms with a reduction in the CHIKV RNA copy number. This was supported by the reduction of E1 RNA and E2 protein in different tissues, including muscle, liver, kidney, and spleen. The reduction in arthritic symptoms, viral RNA copy number, and protein were well supported by the survival curve. The *in vivo* efficacy of TM against CHIKV infection at an acceptable human equivalent dose suggests its suitability for repurposing against this disease. However, it is difficult to extrapolate the preclinical data for clinical application without further clinical validation. Nonetheless, to evaluate its suitability, TM was investigated against CHIKV infection in hPBMC-derived monocyte-macrophage population *in vitro*. While CHIKV infection increased CPE and E2 positive cells, treatment with TM decreased these effects, proving its clinical efficacy.

The *in vitro* findings that were supported by the preclinical data demonstrated the worth of TM to be considered for further investigation for repurposing against CHIKV. Because the AT1/PPAR-$\gamma$/MAPK pathways and downstream mediators are modulated by TM, it might regulate both infection and symptoms of CHIKV (Fig. 10). Because these are host pathways and inflammation is a common etiology in the viral disease progression, TM might have effects against other viruses. In support of this, we found an IC$_{50}$ of 9.78 $\mu$M and 26.3 $\mu$M against herpes simplex virus 1 (HSV-1) and Japanese encephalitis virus (JEV), respectively (data not shown). This is interesting because it also suggests that it has a broad spectrum of antiviral action. In addition, unlike other AT1 blockers, TM has better access to the brain, which makes it suitable for application against viruses affecting the brain, e.g., CHIKV and JEV. However, it is desirable to reduce the dose of TM by enhancing its bioavailability. Owing to its poor solubility (Biopharmaceutics Classification System [BCS]-II), this may be a challenge (40). Nevertheless, increasing solubility through amorphization, cocrystallization, or other formulation techniques (41) may enhance its bioavailability and permit a lower dose for application as an antiviral.

In conclusion, the antiviral efficacy of TM can be due to its direct and indirect effects on CHIKV targets and host factors. Considering its history of long-term safety and *in vivo* efficacy against CHIKV, it can be repurposed against CHIKV infection after clinical validation.

## MATERIALS AND METHODS

**Virus and cells.** The Indian outbreak strain of CHIKV (IS; accession no. EF210157.2) and CHIKV prototype strain (PS; accession no. AF369024.2) were generous gifts from M.M. Parida (Defense Research & Development Establishment [DRDE], Gwalior, India). Vero cells (African green monkey kidney epithelial cells) and RAW 264.7 cells (mouse monocyte/macrophage cells) were procured from the National Center for Cell Science (NCCS), India. Vero cells were maintained in Dulbecco's modified Eagle's medium, (DMEM; PAN Biotech, Aiden Bach, Germany) supplemented with 10% fetal bovine serum (FBS; PAN Biotech, Aiden Bach, Germany), gentamycin, and penicillin-streptomycin. RAW 264.7 cells were maintained in RPMI 1640 (Gibco RPMI 1640 GlutaMAX; Invitrogen, Cal, US) supplemented with 10% FBS (Gibco FBS; Invitrogen, Cal, US) and
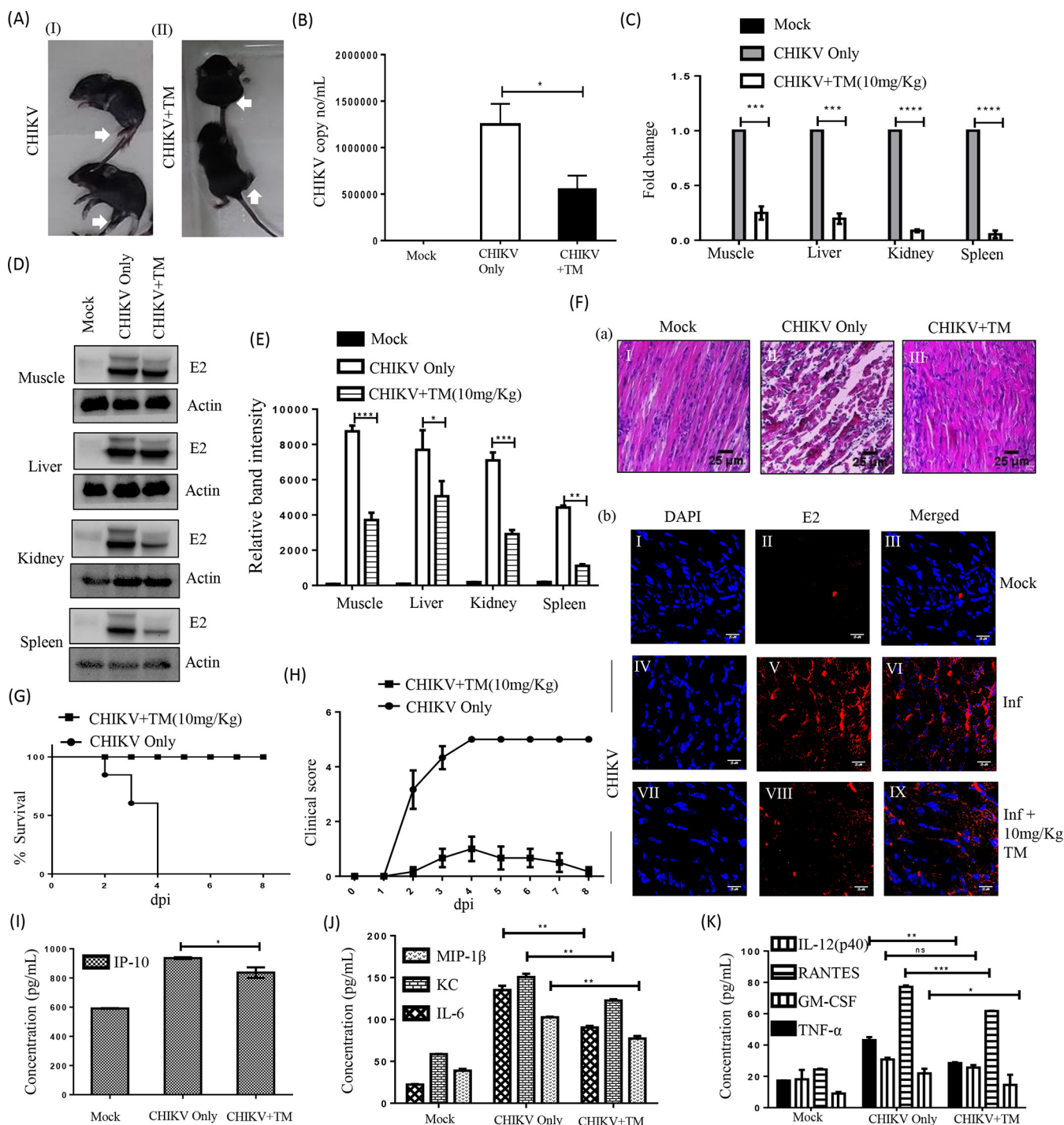
FIG 8 Efficient inhibition of CHIKV infection in mice. C57BL/6 mice were infected subcutaneously with $10^7$ PFU of CHIKV-PS and treated with 10 mg/kg of TM at 12 h intervals up to 4 or 5 d pi. Mice were sacrificed at 5 d pi, and serum and different tissues were collected for further downstream experiments. An equal volume of sera was taken to isolate viral RNA. cDNA was synthesized from an equal volume of viral RNA, and the E1 gene was amplified by qRT-PCR. CHIKV RNA copy number was obtained from a standard curve of Ct value. (A) Image of CHIKV-infected and drug-treated mice. (B) Bar diagram showing CHIKV RNA copy number/ml in virus-infected and drug-treated mice serum. (C) Whole RNA was isolated from the CHIKV-infected and drug-treated samples, and the CHIKV E1 gene was amplified by qRT-PCR. Bar diagram showing the fold change of viral RNA in samples from infected or drug-treated animals. (D) Western blot showing the viral E2 protein in different tissue samples. Actin was used as a loading control. (E) Bar diagram showing the relative band intensities of E2 in samples of different tissues from infected or drug-treated animals. (F) Image panels showing the H&E-stained muscles (a). Image panels showing the CHIKV E2-stained muscles (b). (G) Survival curve showing the efficacy of TM against CHIKV-infected C57BL/6 mice ($n$ = 6/group). (H) Plot showing the disease symptoms during CHIKV infection, which were monitored from 1 d pi to 8 d pi. (I to K) Bar diagrams indicating the concentrations (pg/ml) of different cytokines (IP-10, MIP1-$\beta$, KC, IL-6, IL-12(p40), RANTES, GM-CSF, TNF-$\alpha$) in mock, infected, and drug-treated mice serum. All bar diagrams were obtained through the Graphpad Prism software ($n$ = 3 or $n$ = 6). Data presented as mean $\pm$ SE. $P \leq 0.05$ was considered statistically significant.
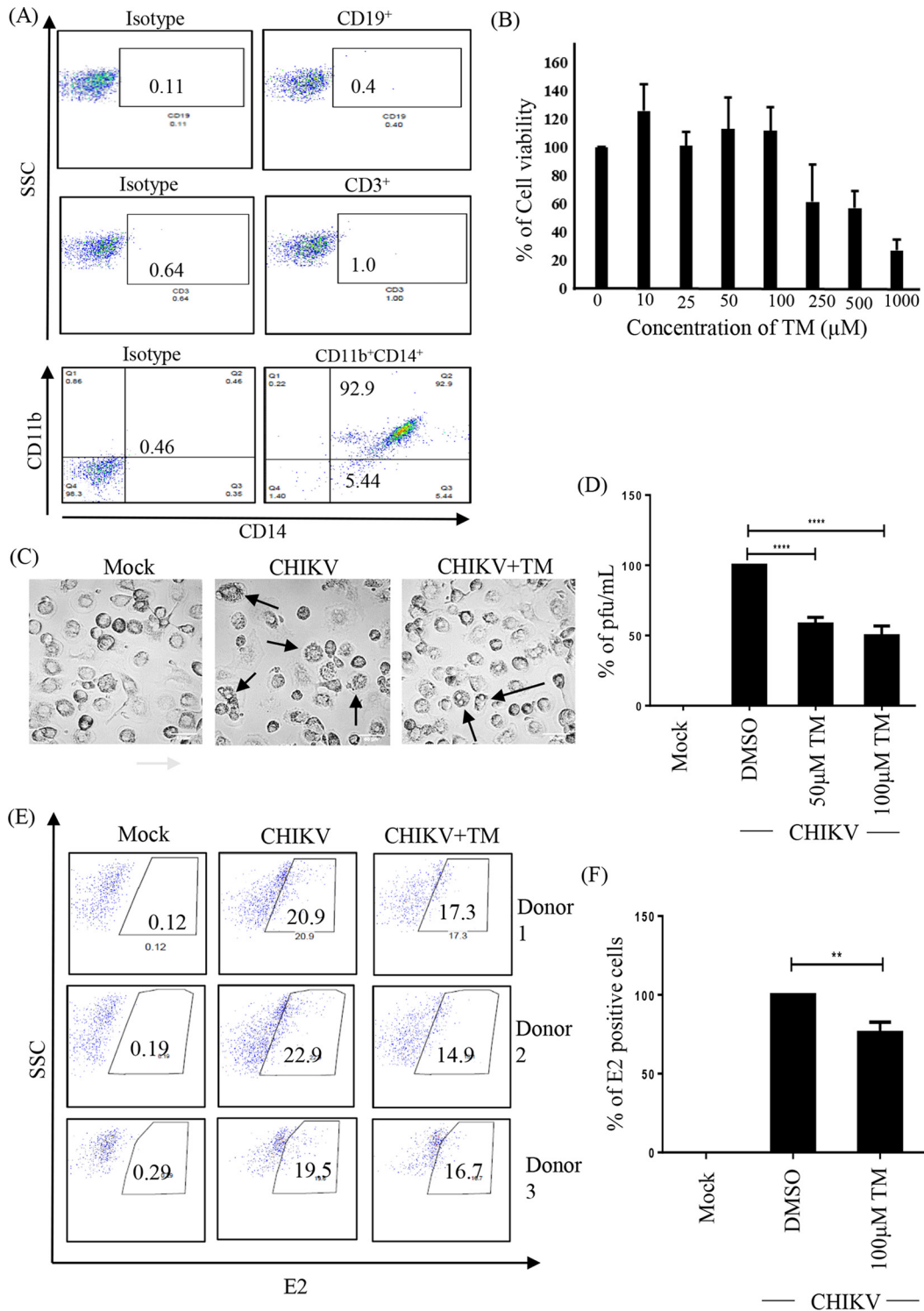
**FIG 9** TM reduces CHIKV infection in hPBMC-derived monocyte-macrophage populations *in vitro*. (A) Dot plot showing the percentages of B cells (CD19), T cells (CD3), and CD14$^+$CD11b+ monocyte-macrophage cells from adherent hPBMCs by flow cytometry. (B) Bar diagram representing the cytotoxicity of TM in hPBMC-derived adherent cell populations by MTT assay. (C) Image showing CHIKV-induced CPE in hPBMC-derived adherent cells. (D) Bar diagram depicting percentage of the viral particle formation obtained by plaque assay. (E) Dot plot showing the percentage of viral E2-positive hPBMC-derived monocyte-macrophage population in mock, CHIKV-infected, and TM-treated CHIKV infection from three healthy donors' hPBMCs obtained using flow cytometry. (F) Bar diagram showing the percentage of positive cells for CHIKV E2 protein, as derived by flow cytometry assay. Data shown are represented as mean $\pm$ SE of three independent experiments. *, $P < 0.05$.
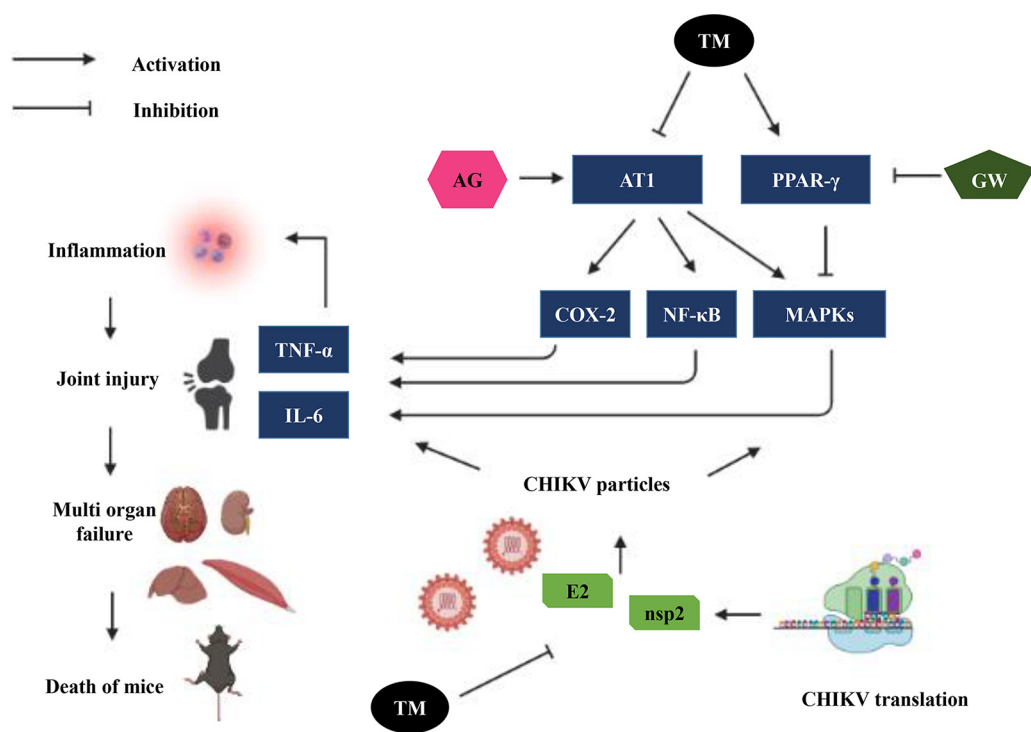
**FIG 10** Schematic representation of proposed working model demonstrating the involvement of AT1, PPAR-γ, and MAPKs after TM treatment during CHIKV infection. Activation of AT1 and blocking of PPAR-γ induced higher phosphorylation of MAPKs with an increase in the expression of COX-2 and NF-κB that led to an increase in the level of inflammatory mediators (TNF-α and IL-6). Infection by CHIKV induced these axes to cause inflammation, tissue injury, and cell death. Both AG and GW increased CHIKV infection and inflammation. TM blocked AT1 and activated PPAR-γ to reduce CHIKV infection and inflammation.

penicillin-streptomycin (PAN Biotech, Aidenbach, Germany). Cells were maintained at 37°C with 5% $CO_2$ in a humidified incubator.

**Antibodies and inhibitors.** The anti-CHIKV E2 monoclonal antibody was a kind gift from M.M. Parida (DRDE, Gwalior, India). The mouse anti-CHIKV nsP2 monoclonal antibody was developed by our group (42). The AT1 monoclonal antibody was procured from Santa Cruz Biotech (TX, US), and the PPAR-γ polyclonal antibody was obtained from Cell Signaling Technology (CST) (MA, US). The antibodies for p38, p-p38, JNK, p-JNK, ERK1/2, p-ERK1/2, p-cJUN, p-IRF3, p-NF-κB, NF-κB, COX-2, were purchased from CST (MA, US). The GAPDH and actin antibodies were purchased from Abgenex India Pvt. Ltd. (Bhubaneswar, India) and Sigma-Aldrich (MO, US) respectively. [Val5]-angiotensin II acetate salt hydrate (Sigma-Aldrich, MO, US) was defined as AG, and GW9662 (Sigma-Aldrich, MO, US) was abbreviated as GW throughout the study. Rosiglitazone (Rosi) and T0070907 (T007) were also procured from Sigma-Aldrich. Telmisartan was a kind gift from Glenmark Life Sciences Ltd., Ankleshwar, Gujrat, India. Fluorochrome conjugated anti-human CD3, CD11b, and CD19 antibodies were obtained from Abgenex, India Pvt. Ltd., and an anti-human CD14 antibody was purchased from eBioscience (CA, US).

**Cytotoxicity assay.** The MTT assay was performed to determine the cytotoxicity of TM, AG, GW, Rosi, and T007 using EZcount™ MTT cell assay kit (Himedia, Mumbai, India) in Vero and RAW 264.7 cells according to the manufacturer's protocol. Approximately 30,000 cells were seeded in 96-well plates 24 h before the experiment. After reaching 70% confluency, cells were treated with increasing concentrations of drugs/inhibitors along with dimethyl sulfoxide (DMSO) as a reagent control. For the cytotoxicity assay, 10 $\mu$L of the MTT reagent (5 mg/mL) was added to the cells 24 h post-drug treatment and incubated for 1 h at 37°C. Next, the medium was removed and 100 $\mu$L of solubilization buffer was added and incubated at 37°C for 15 min to dissolve the Formazan crystals. Finally, the absorbance was measured at 570 nm using a multimode plate reader, and the metabolically active cell percentage was compared with the control cells to determine cellular cytotoxicity (43).

**Virus infection.** At 80% confluency, Vero cells were infected with PS at a MOI of 0.1 and RAW 264.7 cells were infected with IS at a MOI of 5 followed by 90 min incubation with shaking at every 10 to 15 min. After infection, the inoculum was replaced with fresh medium with different concentrations of drugs for 18 h of PS infected Vero cells and 8 h of IS infected RAW 264.7 cells. The harvest time points for the two viral strains of CHIKV were selected based on the previous observations by our group, which indicated that CHIKV-PS produces maximum viral progeny at 18 to 20 h pi whereas CHIKV-IS produces maximum viral progeny at 8 h pi (38, 43). The cytopathic effect (CPE) was observed under a microscope (20× magnification). Infected or TM-treated cells and the supernatants were then harvested to estimate the levels of viral RNA, proteins, and viral titers according to the methods described earlier (44).

**Plaque assay.** Vero cells were seeded in 12-well plates and were infected as described above. Mock, infected, and drug-treated cell supernatants from different experiments were diluted and used for the

infection of fresh Vero cells (70% confluent) seeded in 12-well plates. After 90 min, cells were washed with $1\times$ phosphate-buffered saline (PBS) and overlaid with DMEM containing methylcellulose (Sigma-Aldrich, MO, US) followed by incubation at 37°C with 5% $CO_2$ for 3 to 4 days (d). The cells were then fixed with 8% formaldehyde (Sigma-Aldrich, St. Louis, MO), washed mildly with distilled water, and stained with 0.1% crystal violet (Sigma-Aldrich, St. Louis, MO). The numbers of plaques were counted to calculate the virus titers, which were presented as plaque-forming units per milliliter (PFU/ml) (43).

**Time-of-addition experiment.** After infecting the cells with CHIKV (MOI of 0.1), TM (100 $\mu$M) was added to the cells at 0, 2, 4, 6, 8, 10, 12, 14, and 16 h pi. Ribavirin (10 $\mu$M; Sigma-Aldrich, St. Louis, MO) was used as a control. The supernatants were collected at 18 h pi, and viral titers were determined by plaque assay as described above.

**Treatment before, during, and after infection.** The Vero and RAW 264.7 cells were pretreated with TM (50 $\mu$M) for 3 h. Cells were washed with $1\times$ PBS followed by infection. In case of treatment during the infection, the virus inoculum and TM (50 $\mu$M) were incubated for 30 min and immediately used for infecting the cells for 1.5 h. Following this, cells were washed and fresh media without any drugs was added. For the posttreatment experiment, infected cells were washed, and the drug was added into a fresh medium and introduced to the cells. In the pretreatment experiment, the drug was present before and during the infection. In the posttreatment experiment, the drug was present before, during, and after the infection. Finally, supernatants from the Vero cells and RAW 264.7 cells were collected at 18 h pi and 8 h pi, respectively. Thereafter, the cell supernatant was used in the plaque assay to estimate viral titers.

**Confocal microscopy.** Vero cells were seeded on coverslips in 6-well plates. After reaching 50% confluency, cells were infected as described earlier. At 16 h pi, cells were washed gently thrice with $1\times$ PBS followed by fixation in 4% paraformaldehyde (Sigma-Aldrich, St. Louis, MO) for 30 min at room temperature (RT) and washing with $1\times$ PBS. To permeabilize the cells, 0.5% Triton X-100 (Sigma-Aldrich, St. Louis, MO) was added to each well for 5 min. After three washes, cells were blocked with 3% BSA (Sigma-Aldrich, St. Louis, MO) for 30 min at RT and incubated with a primary antibody of viral protein E2 (1:750) for 1 h. After the primary antibody incubation, secondary anti-rabbit Alexa Flour 594 antibody (Invitrogen, MA, US) was added at 1:1000 and 1:750 dilutions for 45 min. The cells were stained with 4, 6-diamidino-2-phenylindole (DAPI; Life Technology) and mounted with antifade reagent (Invitrogen). The fluorescence microscopic images were acquired using the Leica TCS SP5 confocal microscope (Leica Microsystems, Heidelberg, Germany) with a $20\times$ objective. The images were captured and analyzed using the Leica Application Suite Advanced Fluorescence (LASAF) v.1.8.1 software (45).

**Animal studies.** Animal experiments were conducted strictly under the guidelines defined by the Committee for the Purpose of Control and Supervision of Experiments on Animals (CPCSEA) of India. All procedures and experiments were reviewed and approved by the Institutional Animal Ethics Committee (76/Go/Rebi/S/1999/CPCSEA, 28.02.17). The 10 to 12 d old C57BL/6 mice were bred and housed under specific-pathogen-free conditions at our animal facility. For CHIKV infection, 10 to 12 d old mice were infected with $1 \times 10^7$ PFU of CHIKV-PS subcutaneously at the flank region of the right hind limb. Serum-free medium was injected in the same region to the mock mice. Two hours postinfection, 10 mg/kg TM was given orally to the treated group of mice ($n = 3$). This was continued every 12 h for up to 4 or 5 d postinfection, whereas the mock and infection-control group ($n = 3$) received only solvent. All animals were monitored for disease symptoms every day. On day 5 or 6 pi, depending upon the symptoms, mice were sacrificed, and serum was isolated from the blood. Different tissues were also collected and stored in RNA Later (Invitrogen, MA, US) for RNA isolation, in 10% formalin for histological analysis, or were snap-frozen in liquid nitrogen for Western blot analysis. For the survival curve and clinical score studies, the aforementioned infection and treatment protocols were followed ($n = 6$ mice in three groups). The drug was administered up to 8 d pi. For this study, all mice were monitored every day up to 8 d pi. The clinical score of each mouse was tabulated on daily basis according to the symptom-based disease outcomes (0, no symptoms; 1, fur rise; 2, hunch back; 3, one hind limb paralysis; 4, both hind limb paralysis; 5, death). Mortality was also noted for the survival curve analysis (46).

**qRT-PCR.** Vero cells were seeded onto plates and infected with CHIKV as described above. Viral RNA and supernatants from the infected and treated samples were extracted from the cells. Cells were harvested and RNA extraction was performed using the TRIzol (Invitrogen, MA, US) (43). The cDNA synthesis was carried out with an equal amount of RNA by using the First Strand cDNA synthesis kit (Invitrogen, MA, US), and qRT-PCR was performed using specific primers for the CHIKV E1 and nsP2 genes (Table S1). GAPDH was used as an endogenous control. An equivalent volume of supernatants or serum samples was collected for viral RNA extraction using the QIAamp viral RNA minikit (Qiagen, Hilden, Germany) according to the manufacturer's instructions. An equivalent volume of RNA was used to synthesize cDNA, and the E1 gene was amplified by qRT-PCR with an equivalent volume of cDNA. The Ct values were plotted against the standard curve to obtain the CHIKV RNA copy number (44).

**Western blot.** Protein expression was examined by the Western blot analysis. In brief, virus-infected and drug-treated Vero and RAW 264.7 cells were harvested at different hours postinfection and lysed subsequently with an equivalent volume of radioimmunoprecipitation assay (RIPA) buffer. Snap-frozen tissue samples from the mice were homogenized by a hand homogenizer and lysed in RIPA buffer using the syringe lysis method. Equivalent concentrations of protein were separated on 10% SDS-polyacrylamide gel and were transferred onto a polyvinylidene difluoride (PVDF) membrane (Millipore, MA, US). Next, the membrane was probed with anti-nsP2 (1:1000), anti-E2 (1:2500), anti-AT1 (1:250) monoclonal antibodies, and anti-PPAR-$\gamma$ (1:500) polyclonal antibody. All major MAPKs (p38 polyclonal antibody (pAb), p-p38 pAb, JNK monoclonal antibody (Mab), p-JNK MAb, ERK1/2 MAb, p-ERK1/2 MAb), p-cJUN MAb, p-IRF3 MAb, p-NF-$\kappa$B MAb, NF-$\kappa$B MAb, COX-2 MAb, were used in 1:1000 dilution to probe the membrane. GAPDH monoclonal (1:3000) and actin polyclonal (1:500) antibodies were used as a loading control. Blots were developed by Immobilon Western Chemiluminescent horseradish peroxidase (HRP) substrate (Millipore, MA, US) in ChemiDoc MP Imaging System (Bio-Rad Laboratories, CA, US) and intensities of

all protein bands were quantified from three independent experiments using the Image J software (NIH, Bethesda, MD) (30).

**Flow cytometry.** Flow cytometry was performed as previously described by Mishra et al. (43). In brief, mock, CHIKV-infected, and drug-treated cells were harvested by cellular scrapping. Fixing the cells was performed with 4% paraformaldehyde for 10 min at RT followed by washing with $1\times$ PBS. The cells were then resuspended in fluorescence-activated cell sorter (FACS) buffer ($1\times$ PBS, 1% BSA, 0.01% $NaN_3$ [Sigma-Aldrich, St. Louis, MO]) for staining. Permeabilization buffer ($1\times$ PBS + 0.5% BSA + 0.1% Saponin + 0.01% $NaN_3$) was added to permeabilize the cells for intracellular staining (ICS) of CHIKV antigen. Blocking of the cells was performed by 1% BSA for 30 min at RT. Primary antibodies (anti-mouse nsP2 and E2 MAbs) were then added for 1 h followed by incubation with Alexa Fluor (AF) 488-conjugated chicken anti-mouse antibody (Invitrogen, US). Approximately $1 \times 10^4$ cells were acquired by the LSR-Fortessa flow cytometer (BD Biosciences, CA, US) for each sample and analyzed by the FlowJo software (BD Biosciences, CA, US) (38, 43).

**Sandwich ELISA.** Cell culture supernatants were collected from different experimental sets and stored at $-80°C$. BD OptEIA™ Sandwich enzyme-linked immunosorbent assay (ELISA) kit (San Jose, CA, U.S.A.) was used to determine tumor necrosis factor-alpha (TNF-$\alpha$) and interleukin-6 (IL-6) levels in different test samples according to the previously described protocol (30, 38). The concentrations of cytokines in different test samples were determined with respect to standard curves made from known concentrations of corresponding recombinant cytokines. Epoch 2 (Bio Tek, US) microplate reader was used to determine the cytokine concentrations at 450 nm.

**Histopathological examination.** For histopathological examinations, formalin-fixed tissue samples were dehydrated and embedded in paraffin wax, and serial paraffin sections of 5 $\mu$M were obtained (47). The sections were then stained with hematoxylin and eosin (H&E) (Sigma-Aldrich, St. Louis, MO), and histopathological changes were visualized using a light microscope (Zeiss Vert.A1, Germany). Sections were also examined for the presence of CHIKV E2 protein using a specific antibody. Briefly, an E2 antibody was added to the slides overnight at 4°C. After washing with PBS thrice, slides were incubated with Alexa Fluor 594 (anti-mouse/anti-rabbit; Invitrogen, MA, US) for 45 min at room temperature in the dark. The slides were washed with PBS thrice and then mounted with a mounting reagent using DAPI (Invitrogen, MA, US), and coverslips were applied to the slides (47).

**Measurement of mice cytokines levels.** Serum samples were collected from CHIKV infected and drug-treated 10 to 12 d old C57BL/6 mice at 5 or 6 d pi. The magnetic bead Milliplex kit (Millipore, Billerica, MA, US) was used to measure the levels of cytokines (IL-12(p40), MCP-1, IL-6, IP-10, KC, RANTES, GM-CSF, MIP-1$\beta$, and TNF-$\alpha$) according to the manufacturer's instructions. The plate was read on Luminex-200™ with the xPONENT software (Luminex Corporation, Austin, TX, US) (32).

**Isolation of human peripheral blood mononuclear cells (hPBMCs).** For this, 20 mL blood was collected from three healthy donors in a 50 mL centrifuge tube, rinsed with heparin, and kept on ice until hPBMC isolation. Isolated blood was diluted with an equal volume of chilled $1\times$ PBS (HiMedia, India) followed by vigorous mixing. Two to three milliliters of Hi-Sep LSM (HiMedia, India) were poured in a fifteen-milliliter tube and diluted blood was added in a dropwise and slanted manner up to a final volume of thirteen milliliters per tube followed by centrifugation at 400 relative centrifugal force (RCF) at 25°C for 32 min. Using a Pasteur pipette, a buffy coat was collected and cells were washed with $1\times$ PBS twice at RT at 300 RCF (25°C for 10 min). Isolated PBMCs were plated in 6-well plates (Nunc, Thermo Fischer) at $5 \times 10^6$ cells/well in RPMI 1640 (PAN Biotech) supplemented with 15% FBS (PAN Biotech), antibiotic-antimycotic solution, and ʟ-glutamine (HiMedia, India) for 5 d. The cells were then washed and supplemented with fresh culture medium every 2 d (48, 49).

**Chikungunya virus infection in hPBMCs and flow cytometric staining.** After 5 days, all adherent cells were detached using a cell scraper and seeded in a 24-well plate at a density of $0.15 \times 10^6$ cells. A cytotoxicity assay for TM was carried out for the adherent hPBMCs with various doses of TM by the MTT assay, and more than 95% cell viability was observed ranging up to 100 $\mu$M of TM. After 1 d, adherent cells were pretreated with TM at 100 $\mu$M for 3 h and subjected to CHIKV infection at a MOI of 5 for 2 h. Infected cells were harvested at 12 h pi followed by fixation with 4% paraformaldehyde (PFA). Next, the cells were subjected to intracellular staining to detect viral protein E2 and surface staining for immunophenotyping of adherent population using flow cytometry. For immunophenotyping, fluorochrome-conjugated anti-human CD3, CD11b, CD14, and CD19 antibodies (Abgenex, India) were used (49, 50).

**Statistical analysis.** All the statistical analyses were performed using the GraphPad Prism v. 6.0.1 software. For the animal experiments, differences between the mock, infected, and infected + drug-treated groups were assessed by the one-way ANOVA Dunnett's multiple-comparison test. $P$ values were given as the mean $\pm$ standard error (SE) for $n = 3$ or 6.

**Data availability.** The data that support the findings of this study are available from the corresponding author upon reasonable request. Some data may not be made available because of privacy or ethical restrictions.

## SUPPLEMENTAL MATERIAL

Supplemental material is available online only.
**SUPPLEMENTAL FILE 1**, PDF file, 1.3 MB.

## ACKNOWLEDGMENTS

of Life Sciences (ILS), Bhubaneswar core fund from the DBT, National Institute of Science Education and Research (NISER), Bhubaneswar, Department of Atomic Energy (DAE), Government of India, and School of Pharmaceutical Sciences, Siksha O Anusandhan Deemed to be University, Bhubaneswar. SD was supported by a fellowship from the Council of Scientific and Industrial Research (CSIR), Ministry of Science and Technology, Government of India. The funding agencies did not have any role in the design of the study and collection, analysis, and interpretation of data, and in writing the manuscript.

We declare no conflicts of interest.

This paper adheres to the principles for transparent reporting and scientific rigor of preclinical research as stated in the guidelines for the Design and Analysis, Immunoblotting and Immunochemistry and Animal Experimentation and as recommended by funding agencies, publishers, and other organizations involved in supporting research.

SD, PM, SuC, SoC, and BBS conceived the idea, designed the experiments, and analyzed the results. SuC, SoC, and BBS contributed reagents. SD, SG, SSK, CM, SSP, PM, EL, AR, SC, TM, and SK carried out the experiments. SD, PM, SG, SSK, AR, EL, SS, SuC, SoC, BBS wrote and edited the manuscript. SuC, SoC, and BBS reviewed the manuscript.

## REFERENCES

1. Powers AM. 2015. Risks to the Americas associated with the continued expansion of chikungunya virus. J Gen Virol 96:1–5. https://doi.org/10.1099/vir.0.070136-0.
2. Rougeron V, Sam IC, Caron M, Nkoghe D, Leroy E, Roques P. 2015. Chikungunya, a paradigm of neglected tropical disease that emerged to be a new health global risk. J Clin Virol 64:144–152. https://doi.org/10.1016/j.jcv.2014.08.032.
3. Lima Neto AS, Sousa GS, Nascimento OJ, Castro MC. 2019. Chikungunya-attributable deaths: a neglected outcome of a neglected disease. PLoS Negl Trop Dis 13:e0007575. https://doi.org/10.1371/journal.pntd.0007575.
4. Morrison TE. 2014. Reemergence of chikungunya virus. J Virol 88:11644–11647. https://doi.org/10.1128/JVI.01432-14.
5. Weaver SC, Lecuit M. 2015. Chikungunya virus and the global spread of a mosquito-borne disease. N Engl J Med 372:1231–1239. https://doi.org/10.1056/NEJMra1406035.
6. Cunha RVD, Trinta KS. 2017. Chikungunya virus: clinical aspects and treatment - a review. Mem Inst Oswaldo Cruz 112:523–531. https://doi.org/10.1590/0074-02760170044.
7. Simon F, Javelle E, Cabie A, Bouquillard E, Troisgros O, Gentile G, Leparc-Goffart I, Hoen B, Gandjbakhch F, Rene-Corail P, Franco JM, Caumes E, Combe B, Poiraudeau S, Gane-Troplent F, Djossou F, Schaerverbeke T, Criquet-Hayot A, Carrere P, Malvy D, Gaillard P, Wendling D, Societe de pathologie infectieuse de langue f. 2015. French guidelines for the management of chikungunya (acute and persistent presentations). November 2014. Med Mal Infect 45:243–263. https://doi.org/10.1016/j.medmal.2015.05.007.
8. Ganesan VK, Duan B, Reid SP. 2017. Chikungunya virus: pathophysiology, mechanism, and modeling. Viruses 9:368. https://doi.org/10.3390/v9120368.
9. Mehta R, Gerardin P, de Brito CAA, Soares CN, Ferreira MLB, Solomon T. 2018. The neurological complications of chikungunya virus: a systematic review. Rev Med Virol 28:e1978. https://doi.org/10.1002/rmv.1978.
10. Couderc T, Lecuit M. 2015. Chikungunya virus pathogenesis: from bedside to bench. Antiviral Res 121:120–131. https://doi.org/10.1016/j.antiviral.2015.07.002.
11. Cardona-Ospina JA, Henao-SanMartin V, Paniz-Mondolfi AE, Rodriguez-Morales AJ. 2015. Mortality and fatality due to Chikungunya virus infection in Colombia. J Clin Virol 70:14–15. https://doi.org/10.1016/j.jcv.2015.07.001.
12. Ghildiyal R, Gabrani R. 2020. Antiviral therapeutics for chikungunya virus. Expert Opin Ther Pat 30:467–480. https://doi.org/10.1080/13543776.2020.1751817.
13. Subudhi BB, Chattopadhyay S, Mishra P, Kumar A. 2018. Current strategies for inhibition of chikungunya infection. Viruses 10:235. https://doi.org/10.3390/v10050235.
14. Talevi A, Bellera CL. 2020. Challenges and opportunities with drug repurposing: finding strategies to find alternative uses of therapeutics. Expert Opin Drug Discov 15:397–401. https://doi.org/10.1080/17460441.2020.1704729.
15. Benigni A, Cassis P, Remuzzi G. 2010. Angiotensin II revisited: new roles in inflammation, immunology and aging. EMBO Mol Med 2:247–257. https://doi.org/10.1002/emmm.201000080.
16. Prusty SK, Sahu PK, Subudhi BB. 2017. Angiotensin mediated oxidative stress and neuroprotective potential of antioxidants and AT1 receptor blockers. Mini Rev Med Chem 17:518–528. https://doi.org/10.2174/1389557516666161025094539.
17. Tanaka A, Matsumori A, Wang W, Sasayama S. 1994. An angiotensin II receptor antagonist reduces myocardial damage in an animal model of myocarditis. Circulation 90:2051–2055. https://doi.org/10.1161/01.CIR.90.4.2051.
18. Huang F, Guo J, Zou Z, Liu J, Cao B, Zhang S, Li H, Wang W, Sheng M, Liu S, Pan J, Bao C, Zeng M, Xiao H, Qian G, Hu X, Chen Y, Chen Y, Zhao Y, Liu Q, Zhou H, Zhu J, Gao H, Yang S, Liu X, Zheng S, Yang J, Diao H, Cao H, Wu Y, Zhao M, Tan S, Guo D, Zhao X, Ye Y, Wu W, Xu Y, Penninger JM, Li D, Gao GF, Jiang C, Li L. 2014. Angiotensin II plasma levels are linked to disease severity and predict fatal outcomes in H7N9-infected patients. Nat Commun 5:3595. https://doi.org/10.1038/ncomms4595.
19. Cheng J, Li H, Jie S. 2016. Association of the serum angiotensin II level with disease severity in severe fever with thrombocytopenia syndrome patients. Intern Med 55:895–900. https://doi.org/10.2169/internalmedicine.55.5296.
20. Hernandez-Fonseca JP, Duran A, Valero N, Mosquera J. 2015. Losartan and enalapril decrease viral absorption and interleukin 1 beta production by macrophages in an experimental dengue virus infection. Arch Virol 160:2861–2865. https://doi.org/10.1007/s00705-015-2581-1.
21. Zhang YY, Li JN, Xia HH, Zhang SL, Zhong J, Wu YY, Miao SK, Zhou LM. 2013. Protective effects of losartan in mice with chronic viral myocarditis induced by coxsackievirus B3. Life Sci 92:1186–1194. https://doi.org/10.1016/j.lfs.2013.05.010.
22. Fedson DS, Jacobson JR, Rordam OM, Opal SM. 2015. Treating the Host Response to Ebola Virus Disease with Generic Statins and Angiotensin Receptor Blockers. mBio 6:e00716. https://doi.org/10.1128/mBio.00716-15.
23. Blakely PK, Huber AK, Irani DN. 2016. Type-1 angiotensin receptor signaling in central nervous system myeloid cells is pathogenic during fatal alphavirus encephalitis in mice. J Neuroinflammation 13:196. https://doi.org/10.1186/s12974-016-0683-7.
24. Lewthwaite P, Vasanthapuram R, Osborne JC, Begum A, Plank JL, Shankar MV, Hewson R, Desai A, Beeching NJ, Ravikumar R, Solomon T. 2009. Chikungunya virus and central nervous system infections in children, India. Emerg Infect Dis 15:329–331. https://doi.org/10.3201/eid1502.080902.
25. Tripathi PK, Soni A, Singh Yadav SP, Kumar A, Gaurav N, Raghavendhar S, Sharma P, Sunil SA, Jayaram B, Patel AK. 2020. Evaluation of novobiocin and telmisartan for anti-CHIKV activity. Virology 548:250–260. https://doi.org/10.1016/j.virol.2020.05.010.
26. Nair AB, Jacob S. 2016. A simple practice guide for dose conversion between animals and human. J Basic Clin Pharm 7:27–31. https://doi.org/10.4103/0976-0105.177703.
27. Bassaganya-Riera J, Song R, Roberts PC, Hontecillas R. 2010. PPAR-gamma activation as an anti-inflammatory therapy for respiratory virus infections. Viral Immunol 23:343–352. https://doi.org/10.1089/vim.2010.0016.
28. Brust R, Shang J, Fuhrmann J, Mosure SA, Bass J, Cano A, Heidari Z, Chrisman IM, Nemetchek MD, Blayo AL, Griffin PR, Kamenecka TM, Hughes TS, Kojetin DJ. 2018. A structural mechanism for directing corepressor-selective inverse

agonism of PPARgamma. Nat Commun 9:4687. https://doi.org/10.1038/s41467-018-07133-w.

29. Seargent JM, Yates EA, Gill JH. 2004. GW9662, a potent antagonist of PPARgamma, inhibits growth of breast tumour cells and promotes the anticancer effects of the PPARgamma agonist rosiglitazone, independently of PPARgamma activation. Br J Pharmacol 143:933–937. https://doi.org/10.1038/sj.bjp.0705973.

30. Nayak TK, Mamidi P, Sahoo SS, Kumar PS, Mahish C, Chatterjee S, Subudhi BB, Chattopadhyay S, Chattopadhyay S. 2019. P38 and JNK mitogen-activated protein kinases interact with chikungunya virus non-structural protein-2 and regulate TNF induction during viral infection in macrophages. Front Immunol 10:786. https://doi.org/10.3389/fimmu.2019.00786.

31. Ricciotti E, FitzGerald GA. 2011. Prostaglandins and inflammation. Arterioscler Thromb Vasc Biol 31:986–1000. https://doi.org/10.1161/ATVBAHA.110.207449.

32. Chang AY, Tritsch S, Reid SP, Martins K, Encinales L, Pacheco N, Amdur RL, Porras-Ramirez A, Rico-Mendoza A, Li G, Peng J, Firestein GS, Simon GL, Bethony JM. 2018. The cytokine profile in acute chikungunya infection is predictive of chronic arthritis 20 months post infection. Diseases 6:95. https://doi.org/10.3390/diseases6040095.

33. Varghese FS, Thaa B, Amrun SN, Simarmata D, Rausalu K, Nyman TA, Merits A, McInerney GM, Ng LFP, Ahola T. 2016. The antiviral alkaloid berberine reduces chikungunya virus-induced mitogen-activated protein kinase signaling. J Virol 90:9743–9757. https://doi.org/10.1128/JVI.01382-16.

34. Malik S, Suchal K, Gamad N, Dinda AK, Arya DS, Bhatia J. 2015. Telmisartan ameliorates cisplatin-induced nephrotoxicity by inhibiting MAPK mediated inflammation and apoptosis. Eur J Pharmacol 748:54–60. https://doi.org/10.1016/j.ejphar.2014.12.008.

35. Liu Y, Chen S, Liu J, Jin Y, Yu S, An R. 2020. Telmisartan inhibits oxalate and calcium oxalate crystal-induced epithelial-mesenchymal transformation via PPAR-gamma-AKT/STAT3/p38 MAPK-Snail pathway. Life Sci 241:117108. https://doi.org/10.1016/j.lfs.2019.117108.

36. Pang T, Wang J, Benicky J, Sanchez-Lemus E, Saavedra JM. 2012. Telmisartan directly ameliorates the neuronal inflammatory response to IL-1beta partly through the JNK/c-Jun and NADPH oxidase pathways. J Neuroinflammation 9:102. https://doi.org/10.1186/1742-2094-9-102.

37. Jang C, Kim J, Kwon Y, Jo SA. 2020. Telmisartan Inhibits TNFalpha-Induced Leukocyte Adhesion by Blocking ICAM-1 Expression in Astroglial Cells but Not in Endothelial Cells. Biomol Ther (Seoul) 28:423–430. https://doi.org/10.4062/biomolther.2020.119.

38. Nayak TK, Mamidi P, Kumar A, Singh LP, Sahoo SS, Chattopadhyay S, Chattopadhyay S. 2017. Regulation of viral replication, apoptosis and pro-inflammatory responses by 17-AAG during chikungunya virus infection in macrophages. Viruses 9:3. https://doi.org/10.3390/v9010003.

39. Chirathaworn C, Chansaenroj J, Poovorawan Y. 2020. Cytokines and Chemokines in Chikungunya Virus Infection: protection or Induction of Pathology. Pathogens 9:415. https://doi.org/10.3390/pathogens9060415.

40. Stangier J, Su CA, Roth W. 2000. Pharmacokinetics of orally and intravenously administered telmisartan in healthy young and elderly volunteers and in hypertensive patients. J Int Med Res 28:149–167. https://doi.org/10.1177/147323000002800401.

41. Savjani KT, Gajjar AK, Savjani JK. 2012. Drug solubility: importance and enhancement techniques. ISRN Pharm 2012:195727. https://doi.org/10.5402/2012/195727.

42. Kumar S, Mamidi P, Kumar A, Basantray I, Bramha U, Dixit A, Maiti PK, Singh S, Suryawanshi AR, Chattopadhyay S, Chattopadhyay S. 2015. Development of novel antibodies against non-structural proteins nsP1, nsP3 and nsP4 of chikungunya virus: potential use in basic research. Arch Virol 160:2749–2761. https://doi.org/10.1007/s00705-015-2564-2.

43. Mishra P, Kumar A, Mamidi P, Kumar S, Basantray I, Saswat T, Das I, Nayak TK, Chattopadhyay S, Subudhi BB, Chattopadhyay S. 2016. Inhibition of chikungunya virus replication by 1-[(2-Methylbenzimidazol-1-yl) Methyl]-2-Oxo-Indolin-3-ylidene] amino] thiourea(MBZM-N-IBT). Sci Rep 6:20122. https://doi.org/10.1038/srep20122.

44. Sanjai Kumar P, Nayak TK, Mahish C, Sahoo SS, Radhakrishnan A, De S, Datey A, Sahu RP, Goswami C, Chattopadhyay S, Chattopadhyay S. 2021. Inhibition of transient receptor potential vanilloid 1 (TRPV1) channel regulates chikungunya virus infection in macrophages. Arch Virol 166:139–155. https://doi.org/10.1007/s00705-020-04852-8.

45. Kumar S, Kumar A, Mamidi P, Tiwari A, Kumar S, Mayavannan A, Mudulli S, Singh AK, Subudhi BB, Chattopadhyay S. 2018. Chikungunya virus nsP1 interacts directly with nsP2 and modulates its ATPase activity. Sci Rep 8:1045. https://doi.org/10.1038/s41598-018-19295-0.

46. Dhanwani R, Khan M, Lomash V, Rao PV, Ly H, Parida M. 2014. Characterization of chikungunya virus induced host response in a mouse model of viral myositis. PLoS One 9:e92813. https://doi.org/10.1371/journal.pone.0092813.

47. Priya R, Patro IK, Parida MM. 2014. TLR3 mediated innate immune response in mice brain following infection with Chikungunya virus. Virus Res 189:194–205. https://doi.org/10.1016/j.virusres.2014.05.010.

48. Ziegler-Heitbrock HW, Ulevitch RJ. 1993. CD14: cell surface receptor and differentiation marker. Immunol Today 14:121–125. https://doi.org/10.1016/0167-5699(93)90212-4.

49. Rao SP, Sancho J, Campos-Rivera J, Boutin PM, Severy PB, Weeden T, Shankara S, Roberts BL, Kaplan JM. 2012. Human peripheral blood mononuclear cells exhibit heterogeneous CD52 expression levels and show differential sensitivity to alemtuzumab mediated cytolysis. PLoS One 7:e39416. https://doi.org/10.1371/journal.pone.0039416.

50. Her Z, Malleret B, Chan M, Ong EK, Wong SC, Kwek DJ, Tolou H, Lin RT, Tambyah PA, Renia L, Ng LF. 2010. Active infection of human blood monocytes by Chikungunya virus triggers an innate immune response. J Immunol 184:5903–5913. https://doi.org/10.4049/jimmunol.0904181.